The Block V Receiver Fast Acquisition Algorithm for the Galileo S-Band Mission

M. Aung, W. J. Hurd, C. M. Buu, and J. B. Berner
Radio Frequency and Microwave Subsystems Section

S. A. Stephens
Tracking Systems and Applications Section

J. M. Gevargiz
Telecommunications Systems Section

A fast acquisition algorithm for the Galileo suppressed carrier, subcarrier, and data symbol signals under low data rate, low signal-to-noise ratio (SNR) and high carrier phase-noise conditions has been developed. The algorithm employs a two-arm fast Fourier transform (FFT) method utilizing both the in-phase and quadrature-phase channels of the carrier. The use of both channels results in an improved SNR in the FFT acquisition, enabling the use of a shorter FFT period over which the carrier instability is expected to be less significant. The use of a two-arm FFT also enables subcarrier and symbol acquisition before carrier acquisition. With the subcarrier and symbol loops locked first, the carrier can be acquired from an even shorter FFT period. Two-arm tracking loops are employed to lock the subcarrier and symbol loops with the carrier loop open. In addition, a new method is introduced for loop parameter modification to achieve the final (high) loop SNR in the shortest time possible. The fast acquisition algorithm is implemented in the Block V Receiver (BVR). This article describes the complete algorithm design, the extensive computer simulation work done for verification of the design and the analysis, implementation issues in the BVR, and the acquisition times of the algorithm. In the expected case of the Galileo spacecraft at Jupiter orbit insertion, $P_D/N_o = 14.6$ dB-Hz, $R_{sym} = 16$ symbols per sec, and the predicted acquisition time of the algorithm (to attain a 0.2-dB degradation from each loop to the output symbol SNR) is 38 sec.

I. Introduction

Due to the Galileo high-gain antenna failure, the spacecraft will be transmitting very low data-rate signals with very low signal-to-noise ratios (SNRs). For a significant portion of the mission, including the time of the Jupiter orbit insertion (JOI), the S-band (2.3-GHz) carrier signal will have high phase instability due to solar plasma process noise. Under these conditions, fast acquisition is extremely important both to minimize data loss and because slower acquisition methods fail when the phase is not stable over the (long) acquisition time. An additional complication to the acquisition process is that, for the first time for the Deep Space Network, the received signal modulation type will be a fully suppressed

carrier with a fully suppressed subcarrier, which requires new algorithms. A fast acquisition algorithm for Galileo suppressed carrier, subcarrier, and data symbol signals under low data rate, low SNR, and high carrier phase-noise conditions has been developed. The algorithm is implemented in the Block V Receiver (BVR) [1] and is under consideration for implementation in the buffered telemetry demodulator (BTD). This article describes the complete algorithm design. Details of the various algorithms are given in the referenced internal memoranda and will be published in future issues of this report.

A. The Approach

The approach of the fast acquisition algorithm is to implement nonlinear detection algorithms to generate signals with sinusoidal components related to the subcarrier, symbol, and suppressed carrier signals, and then to estimate the signal frequencies and phases from the signals via fast Fourier transform (FFT) methods. This part of the fast acquisition algorithm will be referred to as the FFT acquisition. The corresponding tracking loops are then closed with initial frequencies and phases set to the FFT-estimated values. Each tracking loop is closed with a minimal initial loop SNR, and the final (high) loop SNR, necessary for negligible output-symbol SNR loss, is achieved by gradually narrowing the loop bandwidth (and transition window width if applicable) to final values resulting in the low SNR loss. (The transition window in the subcarrier and symbol loops is the window region about the data transition that is integrated [2]. The window has a value in the range (0,1]. Windowing is implemented for noise reduction whenever square signals are tracked. Hence, windowing is used for subcarrier and symbol tracking, but not for carrier tracking.) This part will be referred to as the loop acquisition. Therefore, the fast acquisition algorithm can be described as a composition of two parts: the FFT acquisition and the loop acquisition.

Multiple novel enhancement methods were incorporated into the fast acquisition algorithm design to acquire the subcarrier, symbol, and suppressed carrier in a much shorter acquisition time than if using the existing methods. In the FFT acquisition, a novel combination of the carrier and subcarrier in-phase (I) and quadrature-phase (Q) demodulated signals is utilized. This approach reduces the number of symbols required for the FFT at the required SNR by a factor of two. The new signals are a combination of all four II, IQ, QI, and QQ, where the II, IQ, QI, and QQ are the I and Q carrier and subcarrier demodulated signals as shown in Fig. 1, instead of the traditional combination of only two signals. Using a complex FFT results in a single-tone, sign-correct frequency estimate. Therefore, further testing for the polarity of the frequency estimate is eliminated. In frequency estimation from the FFT, a sinc interpolation method (Appendix) is used that results in refined estimates of the frequency and phase.

In loop acquisition, a new approach to the entire loop acquisition process, from choosing the initial bandwidth and window values through narrowing these parameters at the fast rate, is introduced. Also, due to the design to initialize both the phase and frequency of the tracking loops with refined (FFT) estimates, the loops start out essentially in lock immediately after closure. An additional advantage of the loop starting in lock is that the bandwidth and window narrowing process can be activated immediately after loop closure.

A new approach to suppressed carrier acquisition is employed when the carrier phase noise is high. In this case, the subcarrier and symbol are acquired first with the carrier loop open, which can be done because the subcarrier and symbol signals have lower phase noise due to the lower frequencies relative to the carrier. This approach of first acquiring the subcarrier and symbol is taken because, when the subcarrier tracking loop (SCL) and symbol synchronization loop (SSL) are locked, the SNR loss in the carrier acquisition FFT is significantly reduced, resulting in a shorter acquisition FFT time requirement during which the effects of high carrier phase noise are expected to be less significant.

Two-arm SCL and SSL have been introduced for tracking the subcarrier and symbol with the carrier loop open. The two-arm loops (which use both the carrier I and Q arms) provide a 3-dB gain over the traditional one-arm loops in the low SNR case (to be reported on in a future article of this report). When

the carrier loop is closed, only additional noise is introduced by the use of the second arm; therefore, the conventional one-arm SCL and SSL are used.
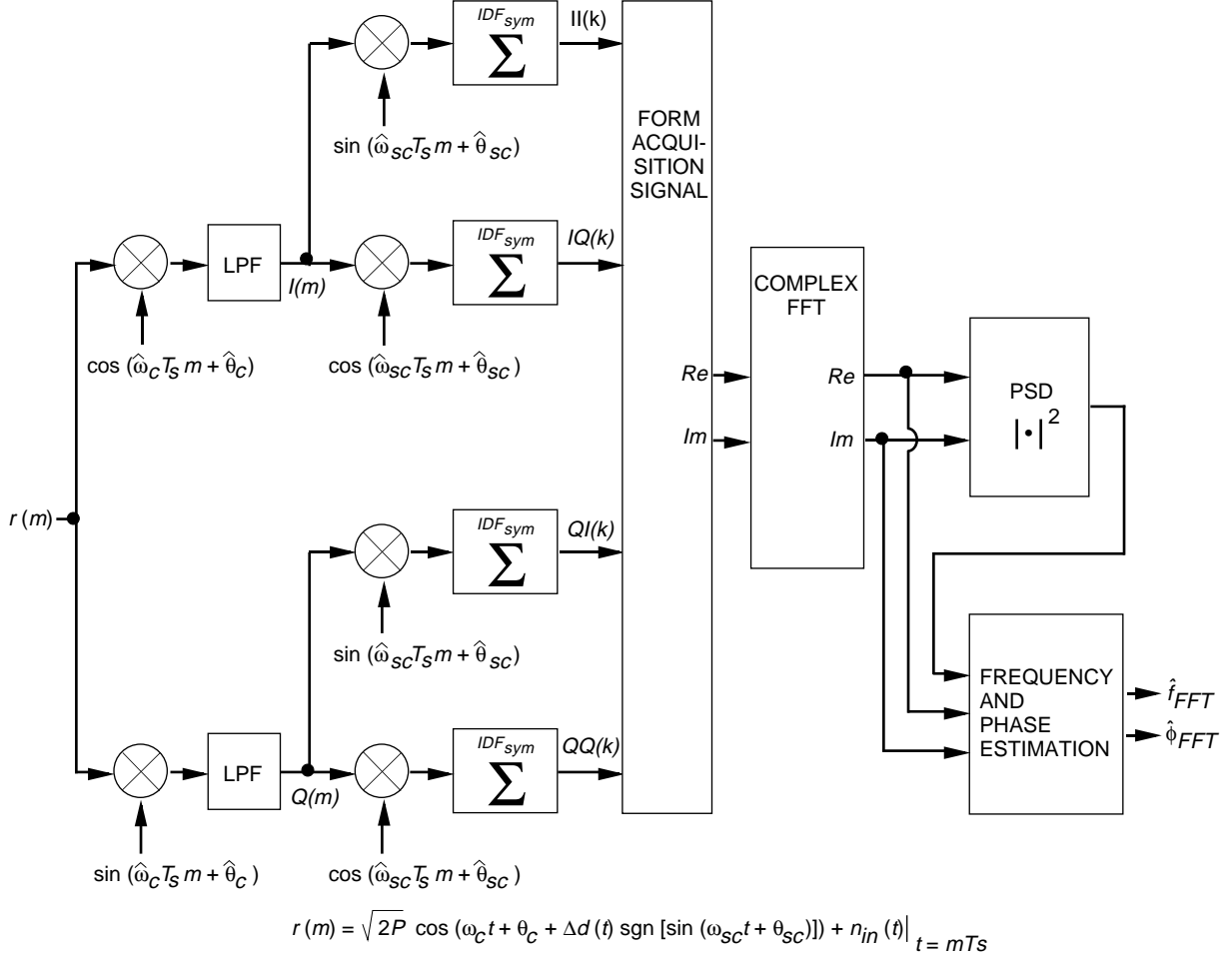

$$r(m) = \sqrt{2P} \, \cos(\omega_c t + \theta_c + \Delta d(t) \, \text{sgn}[\sin(\omega_{sc} t + \theta_{sc})]) + n_{in}(t)\big|_{t=mTs}$$

Fig. 1. FFT-acquisition setup for the fast acquisition algorithm in the BVR.

B. Outline

In Section II, the fast acquisition algorithm process is described. In Section III, the FFT acquisition algorithm is described. The loop acquisition is described in Section IV. In Section V, the issues for implementing the algorithm in the Block V Receiver are discussed. Results of computer simulations are presented in Section VI. Finally, in Section VII, the acquisition times of the algorithm are presented.

II. Algorithm Flowchart

The flows of the algorithm are shown in Figs. 2 and 3 for two cases: when the carrier phase noise is high and when it is low, respectively.

A. Algorithm Flowchart When Carrier Phase Noise Is High

For a significant portion of its mission, the Galileo spacecraft is expected to have high carrier phase noise (e.g., the carrier phase and frequency can be moved significantly during the initial acquisition FFT time due to solar plasma). In this case, the subcarrier and symbol, which are relatively more stable due to lower frequencies relative to the carrier, are acquired first. By doing so, losses to the carrier acquisition

signal due to the subcarrier and symbol are reduced. One source of loss is from the fact that, before subcarrier acquisition, only the first harmonic of the subcarrier signal is captured for the FFT acquisition, compared to after subcarrier acquisition when all the harmonics are captured. Additional losses arise from the subcarrier and symbol phase errors. After reduction of the subcarrier and symbol losses, the SNR in the carrier acquisition is enhanced. As a result, a shorter acquisition time is required for the carrier acquisition FFT, during which the effects of the carrier dynamics are expected to be less significant.

For this case, the flowchart of the acquisition algorithm is shown in Fig. 2. Step (1) will be to FFT-acquire the subcarrier. The subcarrier is acquired using $N_{sc,acq}$ FFTs with $N_{sc,acq}$ different, equally spaced symbol phase offsets. We use $N_{sc,acq}$ symbol phase offsets so that losses due to symbol phase error are minimized if the error in predicted symbol rate is small (Section III.A). In step (2), subcarrier acquisition is verified (see Section III.D). If the subcarrier was not acquired, a larger FFT size will be determined in step (9), and the acquisition process restarts from step (1).

After subcarrier FFT acquisition, a decision is made if the symbol rate is known accurately. For automating this decision, a method utilizing the relationship between the amplitudes of the $N_{sc,acq}$ subcarrier acquisition FFTs is currently under development. If the symbol rate is known, symbol phase is estimated via interpolation of the subcarrier acquisition FFTs [step (4)]. If the symbol rate is not known, the symbol frequency and phase are estimated via an FFT approach [step (11)]. For the symbol acquisition FFT, the data stored from the subcarrier FFT acquisition are reused after refitting the stored data with the FFT-estimated subcarrier phase error. If a longer data set is required for symbol acquisition, the stored data set will be complemented with consecutively collected new data. By mainly using the stored data, little or no additional time is required for data collection [step (10)].

After estimation of the subcarrier and symbol frequency and phase via the FFT acquisition, the SCL and the SSL are initialized with the FFT-estimated frequencies and phases and closed. The bandwidth and window narrowing process is started immediately [steps (5) and (6)]. Note that the initial phase used to start the loop is the phase estimated for time $t = t_{cl,loop}$, the time at which the loop is closed. The subcarrier loop is closed with a square subcarrier reference; hence, all harmonics of the square wave are used after this point. Because the subcarrier and symbol are tracked while the carrier is open, two-arm SCL and SSL are used, which provide a 3-dB gain over the one-arm loops in the low SNR case.

Next, the carrier is FFT acquired [step (7)]. New data can be collected for this step immediately after the subcarrier and symbol loops are closed, as these loops are then assumed to be in lock. Finally, when the carrier is FFT-acquired successfully, the carrier tracking loop will be initiated with the estimated frequency and phase and closed, and the bandwidth narrowing process will be started immediately [step (8)].

B. Algorithm Flowchart When the Carrier Phase Noise Is Low

The flowchart of the acquisition algorithm when the carrier phase noise is relatively low, e.g., when the Sun–Earth–probe (SEP) angle is large, is shown in Fig. 3. In this case, the carrier frequency and phase are expected to be stable for the duration of the longer initial FFT time. (Recall that a long FFT time is required without the subcarrier and symbol lock, i.e., with the losses from using only the first harmonic of the subcarrier and from the subcarrier and symbol phase errors.) Then, the carrier and the subcarrier can be acquired simultaneously [step (1)]. (The acquisition signals for the carrier and the subcarrier are formed from analogous combinations of the same set of II, IQ, QI, and QQ and have the same detection statistics.) The rest of the flowchart is analogous to that for the case of a high carrier phase noise. Note that in step (9) both the carrier and subcarrier errors estimated from FFT acquisitions are refitted to the stored data from step (1).
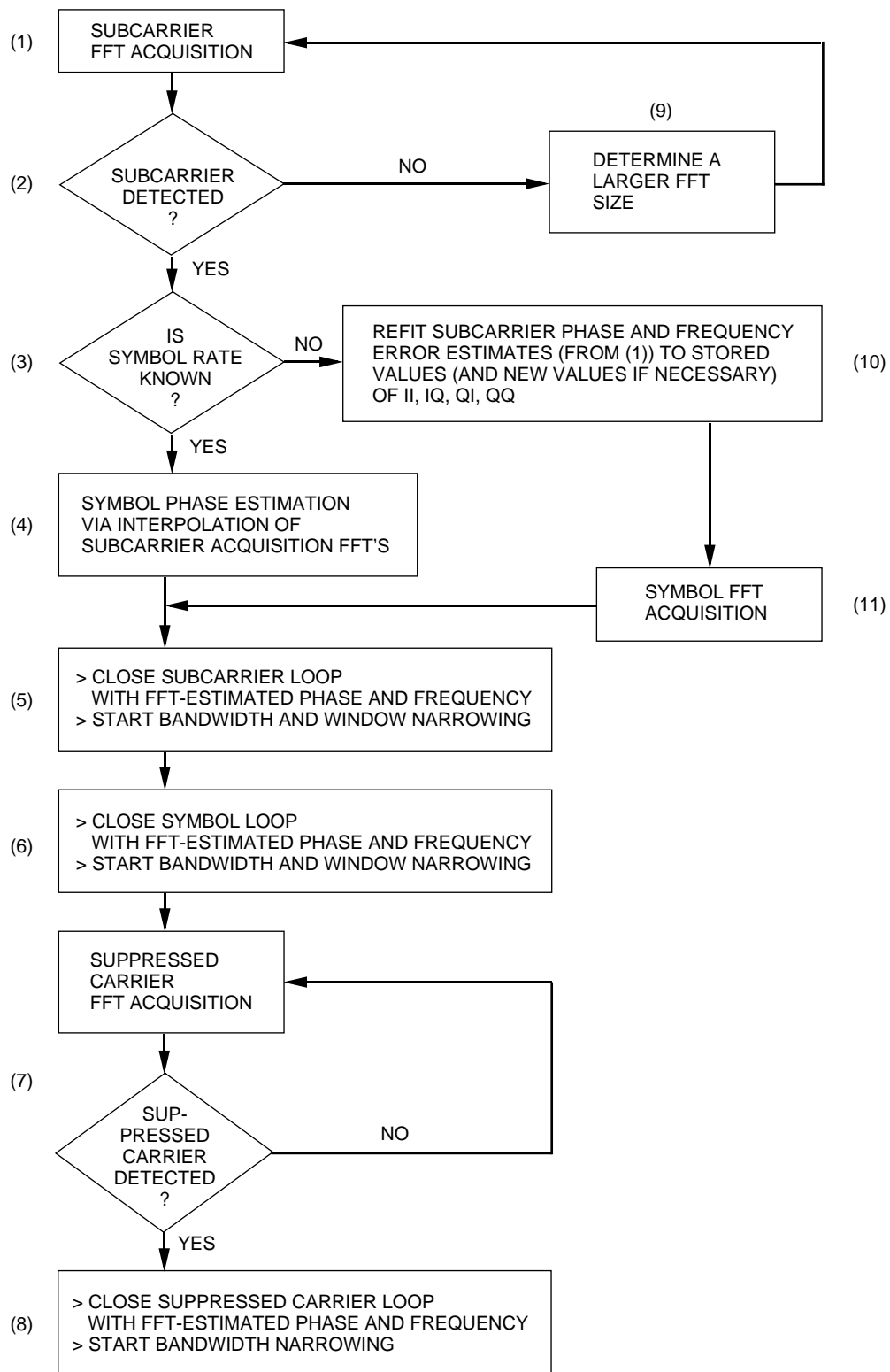
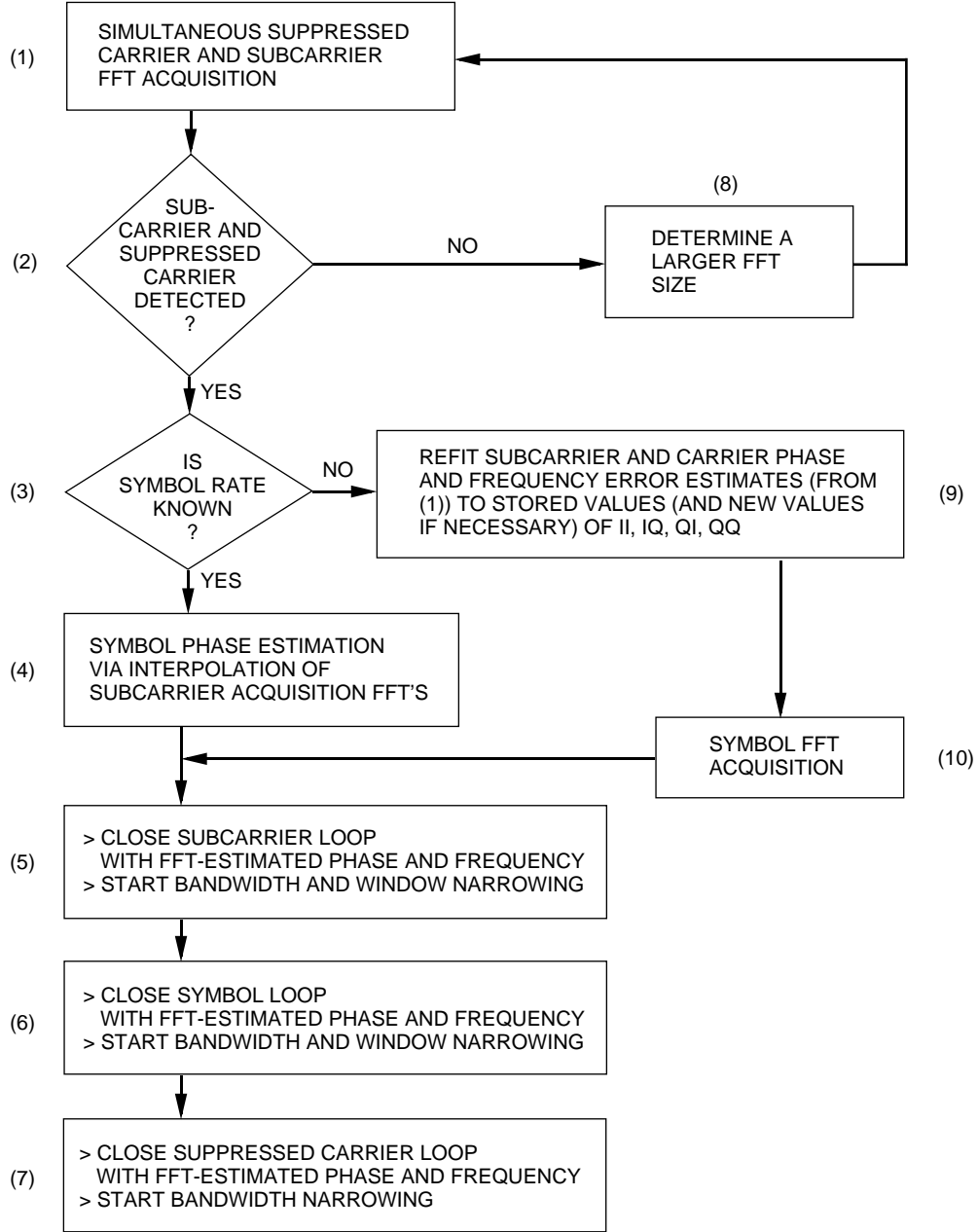**Fig. 2. Algorithm flowchart when the carrier phase noise is high.**

Fig. 3. Algorithm flowchart when the carrier phase noise is low.

III. FFT Acquisition

In this section, the FFT acquisition component of the fast acquisition algorithm is discussed. The setup of the receiver for the FFT acquisition is shown in Fig. 1. The input signal is modeled to be

$$r(m) = \sqrt{2P}\cos\left(\omega_c t + \theta_c + \Delta d(t)\, \text{sgn}\left[\sin\left(\omega_{sc}t + \theta_{sc}\right)\right]\right) + n_{in}(t)\,|_{t=mT_s} \tag{1}$$

where

$$\omega_c = 2\pi f_c = \text{carrier frequency}$$

$$\theta_c = \text{carrier phase}$$

$$\Delta = 90 \text{ deg (modulation index for suppressed carrier)}$$

$$d(t) = \text{data symbol of rate } R_{sym} \text{ symbols per sec}$$

$$\omega_{sc} = 2\pi f_{sc} = \text{subcarrier frequency}$$

$$\theta_{sc} = \text{subcarrier phase}$$

$$n_{in}(t) = \text{input noise, modeled as white Gaussian noise in analysis}$$

$$T_s = \text{sampling period of the signal}$$

$$m = \text{sample index corresponding to a sampling period of } T_s \text{ sec}$$

The $I(\cdot)$ and $Q(\cdot)$ signals are defined as

$$I(m) \triangleq r(m)\cos\left(\hat{\omega}_c m T_s + \hat{\theta}_c\right)|_{LPF}$$

$$Q(m) \triangleq r(m)\sin\left(\hat{\omega}_c m T_s + \hat{\theta}_c\right)|_{LPF}$$

where $|_{LPF}$ indicates low-pass filtering, and

$$\hat{\omega}_c = 2\pi \hat{f}_c = \text{predicted carrier frequency used in the carrier numerically controlled oscillator (NCO)}$$

$$\hat{\theta}_c = \text{predicted carrier phase used in the carrier NCO}$$

The II, IQ, QI, and QQ signals are defined as

$$II(k) \triangleq I(m)\sin\left(\hat{\omega}_{sc} m T_s + \hat{\theta}_{sc}\right)|_{IDF_{sym}}$$

$$= AD(k)\sin\left(\phi_{e,c}(k)\right)\cos\left(\phi_{e,sc}(k)\right) + N_{II}(k) \tag{2}$$

$$IQ(k) \triangleq I(m)\cos\left(\hat{\omega}_{sc} m T_s + \hat{\theta}_{sc}\right)|_{IDF_{sym}}$$

$$= AD(k)\sin\left(\phi_{e,c}(k)\right)\sin\left(\phi_{e,sc}(k)\right) + N_{IQ}(k) \tag{3}$$

$$QI(k) \triangleq Q(m)\sin\left(\hat{\omega}_{sc} m T_s + \hat{\theta}_{sc}\right)|_{IDF_{sym}}$$

$$= AD(k)\cos\left(\phi_{e,c}(k)\right)\cos\left(\phi_{e,sc}(k)\right) + N_{QI}(k) \tag{4}$$

$$QQ(k) \triangleq Q(m)\cos\left(\hat{\omega}_{sc} m T_s + \hat{\theta}_{sc}\right)|_{IDF_{sym}}$$

$$= AD(k)\cos\left(\phi_{e,c}(k)\right)\sin\left(\phi_{e,sc}(k)\right) + N_{QQ}(k) \tag{5}$$

where $|_{IDF_{sym}}$ indicates integration over the estimated symbol period $\hat{T}_{sym}$; k is the sample index corresponding to the kth overlapped integration period as shown for $N_{sc,acq} = 4$ in Fig. 4(a), and
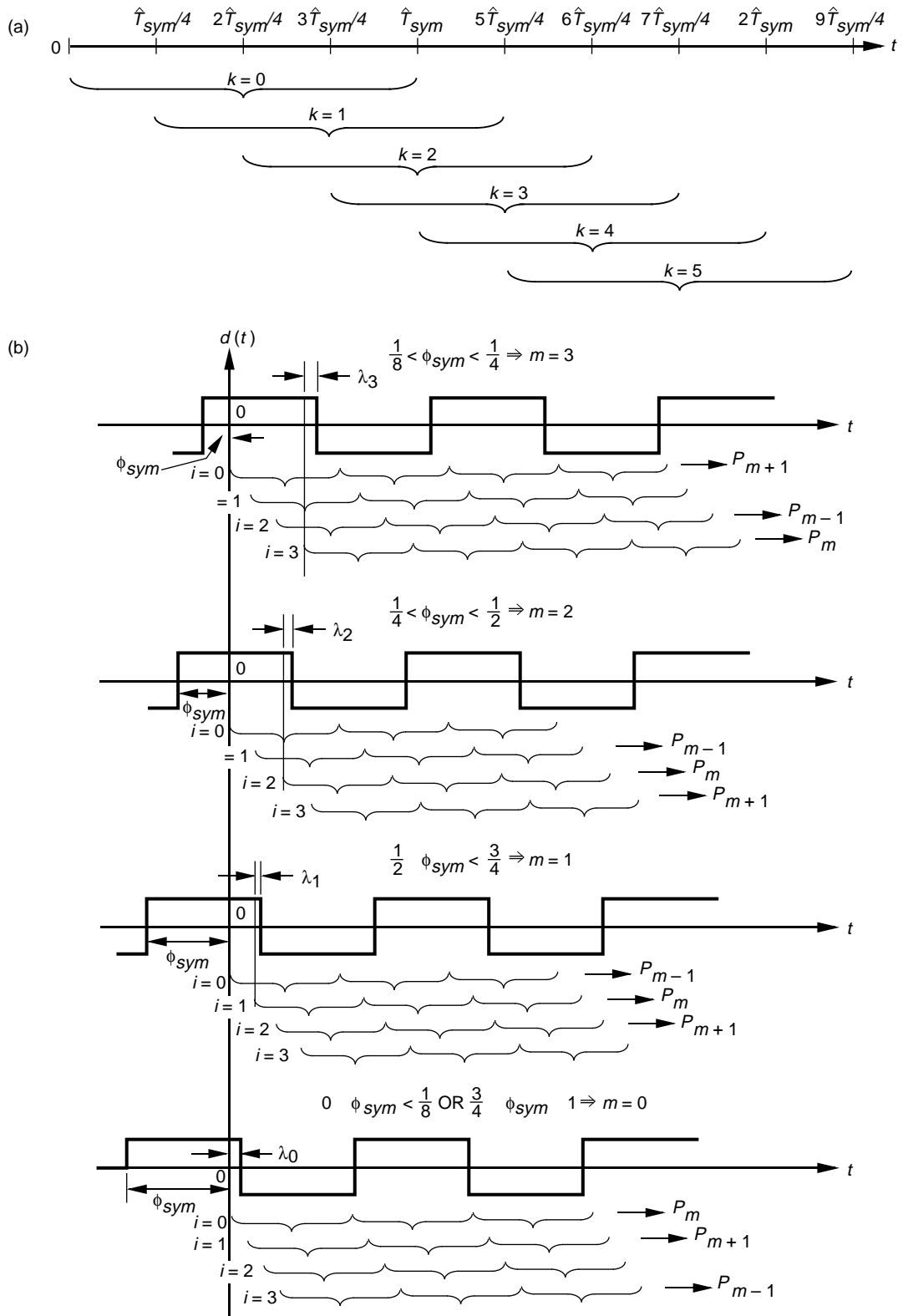
Fig. 4. Symbol acquisition: (a) overlapped integration intervals of II, IQ, QI, and QQ for $N_{sc, acq} = 4$; and (b) relationship between ϕ_{sym} and the symbol integration interval (i) which results in the PSD with the largest peak (P_m).

$$\hat{\omega}_{sc} = 2\pi \hat{f}_{sc} = \text{predicted subcarrier frequency used in the SCL NCO}$$

$$\hat{\theta}_{sc} = \text{predicted subcarrier phase used in the SCL NCO}$$

$$\phi_{e,c}(k) = \text{carrier demodulation error}$$

$$\phi_{e,sc}(k) = \text{subcarrier demodulation error}$$

$$A = -\sqrt{2P}/\pi$$

$$D(k) = \text{the data symbol integrated over the estimated symbol period}$$

Note that to avoid significant degradation due to integration of the signals over the estimated symbol period, $\hat{T}_{sym}$ (in the IDF_{sym} in Fig. 1), the subcarrier and carrier frequency predict errors are required to be much less than the symbol rate. A rule of thumb is to require $\Delta f_{carr-or-sc} < (R_{sym}/20)$ Hz, where $\Delta f_{carr-or-sc}$ is the maximum carrier or suppressed carrier frequency error. Note also that only the first harmonic of the square subcarrier is retained in the I's and Q's.

The first letters in II, IQ, QI, and QQ indicate the in-phase (I) or quadrature-phase (Q) carrier demodulation, and the second letters indicate the I or Q subcarrier demodulation in the receiver. The definition of the I and Q demodulation (whether cosine or sine for I or Q) is arbitrary. A different definition of the I's and Q's leads to a different combination of the I's and Q's in forming the acquisition signals. However, if from end to end the signal definition of the I's and Q's and the combinations of the I's and the Q's are consistent, and if the FFT estimated phase and frequency are applied to the loops with the correct polarization, the final FFT-acquisition result will be the same.

The $II(k)$, $IQ(k)$, $QI(k)$, and $QQ(k)$ are generated for $N_{sc,acq}$ overlapping, shifted integration periods of $\hat{T}_{sym}$ sec. The number of overlapped integrations per symbol, $N_{sc,acq}$, is an arbitrary integer value greater than or equal to 4. In the Block V Receiver, the minimum required value of $N_{sc,acq} = 4$ will be used. Hence, in the remainder of the article, $N_{sc,acq} = 4$ is assumed. For this case, the overlapped symbol integration periods are shown in Fig. 4(a).

The subcarrier, symbol, and suppressed carrier are FFT acquired (as shown in Fig. 1) using the four I's and Q's. The subcarrier, symbol, and suppressed carrier acquisition signals, $X_{sc}(\cdot)$, $X_{sym}(\cdot)$, and $X_{carr}(\cdot)$, are formed from combinations of $II(\cdot)$, $IQ(\cdot)$, $QI(\cdot)$, and $QQ(\cdot)$. From each acquisition signal, a power spectral density (PSD) is formed as the magnitude square of the complex FFT of the signal, and the peak bin with PSD value above the detection threshold and bin location within the range of frequency search is detected (Section III.D). From the peak bin and two bins about it, the frequency and phase (at $t = 0$) of the tone, $\hat{f}_{FFT}$ and $\hat{\phi}_{FFT}$ are estimated using a sinc interpolation method (Appendix). Combining FFT-estimated $\hat{f}_{FFT}$ and $\hat{\phi}_{FFT}$ and predicted $\hat{f}$ and $\hat{\theta}$, refined estimates of the subcarrier, symbol, and suppressed carrier are obtained.

In this section, for the I and Q demodulation setup of the BVR shown in Fig. 1, the acquisition signals are defined for the subcarrier, symbol, and suppressed carrier. For each FFT acquisition, the SNR in the acquisition FFT, SNR_{FFT}, defined as,

$$SNR_{FFT} \triangleq \frac{tone\ power}{noise\ power} \triangleq N_{data} \frac{E_s^*}{N_o} \triangleq N_{data} \frac{E_s}{N_o} S_L \tag{6}$$

is presented. (Note that SNR_{FFT} can be defined as N_{data} times an equivalent symbol SNR, E_s^*/N_o, which is the symbol SNR times a signal degradation factor, S_L, in the acquisition signal.) Also for each case, the variances of the FFT-estimated frequency and phase are given. Finally, the determination of FFT parameters in the FFT acquisition is discussed.

A. Subcarrier FFT Acquisition

Subcarrier acquisition is performed in step (1) of Figs. 2 and 3. At this point of the acquisition, the symbol frequency is assumed to be known, but the symbol phase is unknown. (Note that if ΔR_{sym}, the error in the predicted symbol rate, is not negligible, the SNR of the acquisition FFT will be degraded, resulting in either the subcarrier being detected with a weaker SNR, or not being detected in the first FFT.) For the case in which ΔR_{sym} is negligible, the integration of II, IQ, QI, and QQ over the estimated symbol period will have a constant symbol phase error, λ (in cycles), during the FFT and contribute a loss $\overline{D_\lambda^2}$ in SNR_{FFT}:

$$\overline{D_\lambda^2} = \frac{1}{2}\left[1 + (1 - 2\lambda)^2\right] \tag{7}$$

where $\overline{D_\lambda^2}$ is the expected symbol phase-error loss averaged over symbol probability.

To minimize the loss due to $\overline{D_\lambda^2}$, the subcarrier acquisition signals will be formed for four $(N_{sc,acq})$ symbol phase offsets, 1/4 cycle apart as $X_{sc,0}$, $X_{sc,1}$, $X_{sc,2}$, and $X_{sc,3}$. The SNR_{FFT}'s of $X_{sc,0}$, $X_{sc,1}$, $X_{sc,2}$, and $X_{sc,3}$ will be proportional to $\overline{D_{\lambda_0}^2}$, $\overline{D_{\lambda_1}^2}$, $\overline{D_{\lambda_2}^2}$, and $\overline{D_{\lambda_3}^2}$, respectively, where λ_i $(i = 0, 1, 2, 3)$ is the phase error between the actual input symbol epoch and the ith integration interval. The four symbol offset integration intervals and the λ_i's are shown in Figs. 4(a) and (b). Loss due to $\overline{D_\lambda^2}$ is minimized in the subcarrier acquisition by estimating the subcarrier and frequency from the PSD with the largest peak (minimum value of $\overline{D_\lambda^2}$), i.e., the largest peak out of the four PSDs is detected and the FFT containing the largest peak is used for FFT frequency and phase estimation, $\hat{f}_{FFT}$ and $\hat{\phi}_{FFT}$ (at $t = 0$), respectively.

The four subcarrier FFT acquisition signals, $X_{sc,i}(n)$ (i = 0, 1, 2, 3), with the four equally spaced symbol offsets, are

$$X_{sc,i}(n) = \left(II(i + 4n) + jIQ(i + 4n)\right)^2 + \left(QI(i + 4n) + jQQ(i + 4n)\right)^2 \tag{8}$$

where $n = 0, 1, 2, \cdots, N_{data} - 1$, and N_{data} is the number of data samples in the acquisition FFT. Using Eqs. (2)–(5), these equations reduce to

$$X_{sc,i}(n) = \left(AD(i + 4n)\right)^2 e^{j2\phi_{e,sc}(n)} + n_{sc,i}(n) \tag{9}$$

Each PSD of $X_{sc,i}(n)$ $(i = 0, 1, 2, 3)$ will have a peak tone at the bin closest to twice the error in the predicted frequency, i.e., the frequency estimated from the FFT (as in the Appendix), $\hat{f}_{FFT}$, is

$$\hat{f}_{FFT} \approx 2(f_{sc} - \hat{f}_{sc}) \tag{10}$$

where $\hat{f}_{sc}$ is the predicted subcarrier frequency. Similarly, the FFT-estimated phase, $\hat{\phi}_{FFT}$ (estimate of phase at $t = 0$, as in the Appendix), is doubled:

$$\hat{\phi}_{FFT} \approx 2(\theta_{sc} - \hat{\theta}_{sc}) \tag{11}$$

Therefore, the estimate of subcarrier frequency and phase are

$$\hat{f}_{sc,FFT} = \hat{f}_{sc} + \frac{\hat{f}_{FFT}}{2} \tag{12}$$

$$\hat{\phi}_{sc,FFT}(t) = \hat{\theta}_{sc} + \frac{\hat{\phi}_{FFT}}{2} + 2\pi\hat{f}_{sc,FFT}t \tag{13}$$

This new method of combining all four II, IQ, QI, and QQ (using both I and Q channels of the carrier) in the FFT-acquisition signal, instead of the traditional use of only the carrier Q channel, results in a 3-dB improvement in the SNR_{FFT}. Hence, the number of data points necessary to attain a given SNR_{FFT} is reduced by a factor of two. Furthermore, the frequency error estimate is sign correct, eliminating the need to further test for the polarity of the estimated frequency value.

The SNR in each of the subcarrier acquisition FFTs is as follows:[1]

$$SNR_{FFT,i} = N_{data}\frac{E_s}{N_o}S_{L,bin}\frac{(\frac{2}{\pi})^4(\overline{D_{\lambda_i}^2}S_{L,\Delta f})^2}{2\left[(\frac{2}{\pi})^2\overline{D_{\lambda_i}^2}S_{L,\Delta f} + \frac{1}{2(E_s/N_o)}\right]} \tag{14}$$

where

$N_{data} =$ number of symbols in the FFT

$\dfrac{E_s}{N_o} \triangleq \dfrac{P_D T_{sym}}{N_o}$ (symbol SNR)

$\overline{D_{\lambda_i}^2} =$ symbol integration loss in the ith FFT, Eq. (7)

$S_{L,bin} =$ power loss due to the tone not falling exactly on an FFT bin[2]

$\quad = \dfrac{1}{N_{data}^2}\dfrac{\sin^2(\pi\Delta_{bin}/\alpha)}{\sin^2(\pi\Delta_{bin}/(\alpha N_{data}))} \approx \dfrac{\sin^2(\pi\Delta_{bin}/\alpha)}{(\pi\Delta_{bin}/\alpha)^2}$

$\Delta_{bin} =$ fractional bin offset between the true tone bin and the peak FFT bin

$\alpha =$ zero-padding factor in the FFT

$S_{L,\Delta f} =$ power loss due to the tone being away from dc

$\quad = \dfrac{\sin^2(\pi\Delta f_{sc}T_{sym})}{(\pi\Delta f_{sc}T_{sym})^2}$

$\Delta f_{sc} = f_{sc} - \hat{f}_{sc}$

The estimated frequency and phase will have the following variances:[3]

[1] The SNRs in the FFT acquisition of the subcarrier and carrier are derived in M. Aung, "Derivation of the SNR's in the Subcarrier and Carrier FFT Acquisition in the Fast Acquisition Algorithm," JPL Interoffice Memorandum 3338-94-054 (internal document), Jet Propulsion Laboratory, Pasadena, California, June 6, 1994.

[2] The $S_{L,bin}, S_{L,\Delta f}$, and FFT frequency interpolation algorithm (Appendix) are derived in S. A. Stephens, "An Analysis of FFT Tone Acquisition," JPL Interoffice Memorandum 335.1-92-14 (internal document), Jet Propulsion Laboratory, Pasadena, California, May 14, 1992.

[3] The variances of the FFT-estimated frequencies and phases, the probability of FFT detection, and the detection threshold are discussed in S. Stephens and M. Aung, "FFT Estimation Variances," JPL Interoffice Memorandum 335.1-94-DRAFT (internal document), Jet Propulsion Laboratory, Pasadena, California, August 1994.

$$\sigma_{f,FFT}^2 \ = \frac{1}{4} \frac{0.16}{T_{FFT}^2} \frac{1}{SNR_{FFT}} \ \mathrm{Hz}^2 \tag{15}$$

$$\sigma_{\phi,FFT}^2(t) \ = (2\pi)^2 \left(\frac{1}{4} \frac{0.01345}{SNR_{FFT}} + \sigma_{f,FFT}^2 \times \left(t - \frac{T_{FFT}}{2} \right)^2 \right) \ \mathrm{rad}^2 \tag{16}$$

B. Symbol Acquisition

After the subcarrier FFT acquisition, it is determined if the error in the predicted symbol rate error, ΔR_{sym}, is negligible. If so, only the symbol phase is estimated from the subcarrier acquisition FFTs; otherwise, both the frequency and phase are estimated with a new FFT.

1. Determination If Symbol Frequency Is Known Accurately. In step (3) of Figs. 2 and 3, a decision has to be made if the symbol rate is known accurately. If it is not known a priori, a possible method of making this decision is to compare the relative amplitudes of the $N_{sc,acq}$ subcarrier acquisition FFTs. The basic idea is that when the symbol frequency is known, the $N_{sc,acq}$ FFTs will have amplitudes proportional to $D_{\lambda_i}^2$, where λ_i's are phase errors $1/N_{sc,acq}$ cycles apart. On the other hand, when the symbol frequency is not known, the $N_{sc,acq}$ FFTs will have comparable amplitudes. (A method utilizing this principle is under development and will be reported on in a future article.)

2. Symbol Phase Acquisition From Subcarrier Acquisition FFTs. When ΔR_{sym} is negligible, symbol phase can be estimated from the four FFTs with λ_i (i = 0, 1, 2, 3) as follows. In Fig. 4(b), the integration intervals of the input symbol stream, $d(\cdot)$, are shown for integration phase offsets of 0, 0.25, 0.5, and 0.75 cycle (labeled interval index i = 0, 1, 2, and 3, respectively, and λ_i is the phase difference between the input symbol epoch and the ith integration interval). Define m as the interval index of the integration interval that results in the PSD with the largest peak, P_m. It can be seen that m varies depending on the input symbol phase ϕ_{sym} (ϕ_{sym} is defined with respect to the estimated symbol phase $\hat{\phi}_{sym} = 0$ at $t = 0$ at the beginning of the first symbol integration interval), as

$$m = \begin{cases} 3, & \text{if } 1/8 \le \phi_{sym} < 3/8 \text{ cycle} \\ 2, & \text{if } 3/8 \le \phi_{sym} < 5/8 \text{ cycle} \\ 1, & \text{if } 5/8 \le \phi_{sym} < 7/8 \text{ cycle} \\ 0, & \text{otherwise} \end{cases}$$

Index m for various values of ϕ_{sym} is shown in Fig. 4(b), where the label P_m is used to indicate the integration interval that results in the PSD with the largest peak.

Hence, the symbol phase at $t = 0$ (with respect to the integration interval $i = 0$) can be estimated as

$$\hat{\phi}_{sym,FFT}(0) = \left(1 - \frac{m}{4} \right) + \hat{\lambda}_m \tag{17}$$

where $\hat{\lambda}_m$ is the estimate of λ_m, the phase error between the input symbol epoch and the integration interval m. One derives $\hat{\lambda}_m$ by writing the peak amplitudes of the four PSDs (P_i, i = 0, 1, 2, 3) as being proportional to $D_{\lambda_i}^2$, which is a quadratic function of λ_i [Eq. (7)]. Using the quadratic relationship plus the additional information that phase errors λ_i's (i = 0, 1, 2, 3) are one-quarter of a cycle apart, λ_m is estimated as[4]

---

[4] Details of symbol phase estimation and FFT phase estimation discussed in the Appendix are available in M. Aung and S. Stephens to E. W. Stone, "Fast Acquisition Algorithm Developed for the Block V Receiver Support of the Galileo Low Data-rate Mission," JPL Interoffice Memorandum 3338-93-167 (internal document), Jet Propulsion Laboratory, Pasadena, California, August 25, 1993.

$$\hat{\lambda}_m = \frac{b + \sqrt{b^2 - 4ac}}{2a} \qquad (18)$$

where

$$a = 4d$$

$$b = -4\left(1 - \frac{2}{N_{sc,acq}}g\right)$$

$$c = \left(1 + \left(1 - \frac{2}{N_{sc,acq}}g\right)^2\right)d$$

$$d = \frac{\sqrt{P_{m+g}} - \sqrt{P_{m-g}}}{\sqrt{P_{m+g}} + \sqrt{P_{m-g}}}$$

$$P_l = \text{peak value of the } l\text{th PSD}$$

$$g = floor\left[\frac{N_{sc,acq}}{4}\right]$$

In summary, for this case, the estimated symbol parameters are

$$\hat{f}_{sym,FFT} = R_{sym,pred} \qquad (19)$$

$$\hat{\phi}_{sym,FFT}(t) = \hat{\phi}_{sym,FFT}(0) + 2\pi\hat{f}_{sym,FFT}t \qquad (20)$$

The variance of the estimated phase will be approximately

$$\sigma^2_{\phi,FFT} \approx \frac{(2\pi)^2}{16 \times SNR_{FFT}} \text{ rad}^2 \qquad (21)$$

where SNR_{FFT} is the SNR in the subcarrier acquisition FFT given in Eq. (14).

3. Symbol FFT Acquisition When R_{sym} Is Unknown. When the symbol rate is not known, the symbol frequency and phase are estimated from one FFT of the acquisition signal. The acquisition signal is formed using the I's and Q's stored from the subcarrier acquisition, complemented with consecutively collected data if a larger number of symbols are required. Because most or all of the data are already available, little or no addition data collection time is required. Note from Eqs. (2)–(5) that the stored I's and Q's have subcarrier and carrier demodulation error, $\phi_{e,c}$ and $\phi_{e,sc}$, respectively. Using estimates of these demodulation errors available from the subcarrier FFT acquisition (and carrier FFT acquisition if performed prior to symbol acquisition), the errors in the stored data are demodulated out before the data are used for the symbol acquisition signal.

The overview of the algorithm is given here.[5] The approach is to form a signal $X_{sym}(n)$ (for $n = 0, 1, 2, \cdots, N_{data} - 1$) proportional to $D^2(i + 4n)$ ($i = 0, 1, 2,$ or 3) that can be shown to be periodic with

---

[5] Details of the algorithm and the SNR in the FFT are given in M. Aung to E. W. Stone, "FFT Acquisition of Symbol Frequency and Phase After Subcarrier Acquisition With the Carrier Loop Open in the Fast Acquisition Algorithm," JPL Interoffice Memorandum 3338-94-075 (internal document), Jet Propulsion Laboratory, Pasadena, California, July 19, 1994, and in M. Aung to E. W. Stone, "FFT Acquisition of Symbol Frequency and Phase After Carrier and Subcarrier Acquisition in the Fast Acquisition Algorithm," JPL Interoffice Memorandum 3338-94-076 (internal document), Jet Propulsion Laboratory, Pasadena, California, July 19, 1994.

a frequency equal to ΔR_{sym} Hz [Fig. 4(a)]. Therefore, the FFT of $D^2(i + 4n)$ returns harmonic tones at $l\Delta R_{sym}$ ($l = 0, 1, 2, \cdots$), and the frequency and phase can be estimated (Appendix) from the first harmonic. To eliminate the sign ambiguity in the frequency estimate, a complex FFT is formed from the signal and its quadrature as

$$X_{sym,z}(n) = X_{sym,I}(n) + jX_{sym,Q}(n) \tag{22}$$

For $N_{sc,acq} = 4$, it can be shown [Fig. 4(a)] that

$$X_{sym,z}(n) = X_{sym}(n+1) + jX_{sym}(n) \tag{23}$$

because the sequence $X_{sym,I}(n) \triangleq X_{sym}(n+1)$ is in quadrature with the sequence $X_{sym,Q}(n) \triangleq X_{sym}(n)$, as they differ by 90 deg in phase, as shown in Fig. 4(a).

A further modification is added to the algorithm where the acquisition signal is formed as $X_{sym}(n)$ proportional to $D^2(n)$. Then, note from Fig. 4(a) that the consecutive samples of $X_{sym}(n)$ have overlapping integration intervals. The outcome of overlapping is an improvement in the FFT SNR, and the estimated frequency and phase are

$$\hat{f}_{sym,FFT} = \hat{f}_{FFT} \tag{24}$$

$$\hat{\phi}_{sym,FFT}(t) = \hat{\phi}_{FFT} + 2\pi\hat{f}_{sym,FFT}t - \frac{\pi}{2} \tag{25}$$

where $\hat{f}_{FFT}$ and $\hat{\phi}_{FFT}(t)$ are the frequency and phase estimates from the FFT of the acquisition signal $X_{sym}(k)$.

4. Case A: Symbol FFT Acquisition, Retrofitting Only the Subcarrier. When the symbol FFT acquisition is performed after the subcarrier is acquired, with the carrier loop still open [Fig. 2, steps (10) and (11)], the estimated subcarrier frequency and phase errors are rotated out from each sample of the stored I's and Q's, and the acquisition signal is formed as

$$
\begin{aligned}
X_{sym}(n) &= \mid Re\left\{ (QI(n) + jQQ(n))e^{-j\hat{\phi}_{e,sc}(n)} \right\} + jRe\left\{ (II(n) + jIQ(n))e^{-j\hat{\phi}_{e,sc}(n)} \right\} \mid^2 \\[2mm]
&= \left\{ QI(n)\cos\left(\hat{\phi}_{e,sc}(n)\right) + QQ(n)\sin\left(\hat{\phi}_{e,sc}(n)\right) \right\}^2 \\[2mm]
&\quad + \left\{ II(n)\cos\left(\hat{\phi}_{e,sc}(n)\right) + IQ(n)\sin\left(\hat{\phi}_{e,sc}(n)\right) \right\}^2 \\[2mm]
&= A^2 D^2(n)\cos^2\left(\phi_{e,sc}(n) - \hat{\phi}_{e,sc}(n)\right) + n_{sym,FFT} \\[2mm]
&\approx A^2 D^2(n) + n_{sym,FFT}
\end{aligned}
\tag{26}
$$

where $\hat{\phi}_{e,sc}(\cdot)$ is the estimate of the subcarrier demodulation error $\phi_{e,sc}(\cdot)$ in the stored II, IQ, QI, and QQ [Eqs. (2)–(5)], estimated from the subcarrier FFT acquisition.

5. Case B: Symbol FFT Acquisition, Retrofitting the Subcarrier and the Carrier. When symbol acquisition is performed after the subcarrier and the carrier are acquired [Fig. 3, steps (9) and (10)], the symbol frequency and phase are estimated in a manner analogous to case A, with the following acquisition signal. The estimated subcarrier and carrier errors are rotated out from each sample of the stored I's and Q's, and the acquisition signal is

$$X_{sym}(n) = \left(Re\left[e^{-j\hat{\phi}_{e,c}(n)} \left[Re\left\{ (QI(n) + jQQ(n))e^{-j\hat{\phi}_{e,sc}(n)} \right\} + jRe\left\{ (II(n) + jIQ(n))e^{-j\hat{\phi}_{e,sc}(n)} \right\} \right] \right] \right)^2$$

$$= \left(\left[QI(n)\ \cos\ (\hat{\phi}_{e,sc}(n)) + QQ(n)\ \sin\ (\hat{\phi}_{e,sc}(n)) \right]\ \cos\ (\hat{\phi}_{e,c}(n)) \right.$$

$$\left. + \left[II(n)\ \cos\ (\hat{\phi}_{e,sc}(n)) + IQ(n)\ \sin\ (\hat{\phi}_{e,sc}(n)) \right]\ \sin\ (\hat{\phi}_{e,c}(n)) \right)^2 \tag{27}$$

$$= A^2 D(n)^2\ \cos^2\ (\phi_{e,sc}(n) - \hat{\phi}_{e,sc}(n))\ \cos^2\ (\phi_{e,c} - \hat{\phi}_{e,c}) + n_{sym,FFT}$$

$$\approx A^2 D(n)^2 + n_{sym,FFT}$$

where $\hat{\phi}_{e,sc}(\cdot)$ and $\hat{\phi}_{e,c}(\cdot)$ are the estimates of the subcarrier and carrier demodulation errors in the stored data, estimated from the subcarrier and carrier FFT acquisitions.

For cases A and B, the estimated frequencies and phases will have the following variances:

$$\sigma^2_{f,FFT}\ =\ \frac{0.16}{T^2_{FFT}} \frac{1}{SNR_{FFT}}\ \text{Hz}^2 \tag{28}$$

$$\sigma^2_{\phi,FFT}(t)\ =\ (2\pi)^2 \left(\frac{0.01345}{SNR_{FFT}} + \sigma^2_{f,FFT} \times \left(t - \frac{T_{FFT}}{2} \right)^2 \right)\ \text{rad}^2 \tag{29}$$

C. Carrier FFT Acquisition

The suppressed carrier is acquired after the subcarrier and symbol acquisition when the carrier phase noise is high and simultaneously with the subcarrier when the carrier phase noise is low. The carrier acquisition is described for the two cases.

1. Case A: Carrier Acquisition After the Subcarrier and Symbol Have Been Acquired. If the carrier is acquired after the subcarrier and symbol loops are in lock [Fig. 2, step (7)], the carrier frequency and phase are estimated from one FFT. Note that at this point of the acquisition process, the I and Q subcarrier demodulation is performed with square-wave references. The acquisition signal is

$$X_{carr}(n) = \left(QI(4n) + jII(4n) \right)^2 = \frac{P}{2} e^{j2\phi_{e,c}(n)} + n_{carr,acq}(n) \tag{30}$$

The SNR in the FFT will be

$$SNR_{FFT} = N_{data} \frac{E_s}{N_o} S_{L,bin} \frac{S^2_{L,\Delta f}}{8 \left[S_{L,\Delta f} + \frac{1}{2(E_s/N_o)} \right]} \tag{31}$$

2. Case B: Simultaneous Acquisition of the Carrier and the Subcarrier. For simultaneous subcarrier and carrier acquisition [Fig. 3, step (1)], the four carrier FFT acquisition signals are analogous to the subcarrier acquisition signal:

$$X_{carr,i}(n) = \left(QI(i+4n) + jII(i+4n)\right)^2 + \left(QQ(i+4n) + jIQ(i+4n)\right)^2$$

$$= \left(AD(i+4n)^2 e^{j2\phi_{e,c}(n)}\right) + n_{carr,acq}(n) \tag{32}$$

where $i = 0, 1, 2, 3$, and $n = 0, 1, \cdots, N_{data} - 1$. The SNR of the tone in the FFT and the variances of the estimated frequency and phase are the same as those for subcarrier acquisition, given in Eqs. (14)–(16).

Analogous to the subcarrier FFT acquisition, the estimated carrier frequency and phase for both cases A and B are

$$\hat{f}_{c,FFT} = \hat{f}_c + \frac{\hat{f}_{FFT}}{2} \tag{33}$$

$$\hat{\phi}_{c,FFT}(t) = \hat{\theta}_c + \frac{\hat{\phi}_{FFT}}{2} + 2\pi \hat{f}_{c,FFT} t \tag{34}$$

where $\hat{f}_{FFT}$ and $\hat{\phi}_{FFT}$ are the estimates of frequency and phase (at $t = 0$) of the peak tone in the FFT (Appendix), and $\hat{f}_c$ and $\hat{\phi}_c$ are the predicted carrier frequency and phase. The estimated frequency and phase will have the same variance as in Eqs. (15) and (16).

D. Determination of the FFT Parameters

In this section, the FFT parameters, namely N_{data}, detection threshold, and the zero-padding factor, are discussed.

1. Determination of N_{data}. The number of data points to be used in the FFT, N_{data}, is determined from choosing a desired confidence of detection, C, and solving for N_{data}. The confidence of detection, which is the probability of detecting the correct signal bin in the FFT in the presence of noise, is

$$C \approx \left(1 - 0.5 e^{-0.5(E_s^*/N_o)N_{data}}\right)^{2(\Delta f_{search}/R_{sym})N_{data}} \tag{35}$$

where E_s^*/N_o is the equivalent symbol SNR in the acquisition FFT, defined in Eq. (6). The Δf_{search} determines the frequency search region, $\pm \Delta f_{search}$ Hz about the predicted frequency, i.e., the peak bin in the PSD is detected as the bin with the largest PSD value among the bins corresponding to the search frequency range $[\hat{f} - \Delta f_{search}, \hat{f} + \Delta f_{search}]$ Hz. It should be noted that Eq. (35) is only an approximation of the confidence of detection.

2. Detection Threshold. In the FFT acquisition, FFT detection is declared if the peak bin in the search frequency range $[\hat{f} - \Delta f_{search}, \hat{f} + \Delta f_{search}]$ Hz exceeds a lower threshold, P_{thresh}. The lower threshold is set as

$$P_{thresh} \triangleq \xi P_s \tag{36}$$

where

P_s = the expected signal power

$$\xi = \left(1 - \frac{1}{\sqrt{SNR_{FFT}}} Erf^{-1}[2C - 1]\right)^2$$

C = confidence of detection

$Erf^{-1}(\cdot)$ = inverse error function

3. The Zero-Padding Factor. The nominal value of the zero-padding factor, α, will be 4. However, N_{data} is chosen according to Eq. (35), which may not be a 2^n value. In general, the FFT size, N_{FFT}, will be determined as

$$N_{FFT} = 4 \times N_{nearest}$$

where $N_{nearest}$ is the nearest 2^n value greater than or equal to N_{data}. Data points N_{data} plus ($N_{FFT} - N_{data}$) zeros will be used to form the N_{FFT} point FFT. Therefore, the actual zero-padding factor, which should be the value used in all equations requiring α (e.g., frequency interpolation), will be

$$\alpha = \frac{N_{FFT}}{N_{data}} \geq 4 \tag{37}$$

IV. Loop Acquisition

This section discusses loop acquisition. First, initialization of the tracking loop frequency and phase is described. The use of two-arm versus one-arm loops is also briefly discussed, and the majority of the section describes the process of initializing and gradually narrowing the loop bandwidths (and windows if applicable) until the final loop SNR is achieved.

A. Initializing the NCOs of the Tracking Loops

After the FFT acquisition, the (subcarrier, symbol, and carrier if applicable) tracking loops are closed with the FFT estimated parameters. In each loop (indicating subcarrier, symbol, or carrier as $Y =$ "sc," "sym," or "$carr$" in the following), the initial frequency in the numerically controlled oscillator (NCO) is set to $f_{NCO,init}$:

$$f_{NCO,init} = \hat{f}_{Y,FFT} \tag{38}$$

and the initial phase of the NCO is set to $\phi_{NCO,init}$:

$$\phi_{NCO,init} = \hat{\phi}_{Y,FFT}(t_{cl,loop}) \tag{39}$$

where $t = t_{cl,loop}$ is the time at which the loop is closed with respect to $t = 0$ at the beginning of the first symbol integration, shown in Fig. 4(a).

B. Two-Arm and One-Arm Tracking Loops

New two-arm tracking loops have been introduced for subcarrier and symbol tracking while the carrier loop is open. The two-arm loop forms the loop phase error estimate $\hat{\phi}_{e,loop}$ from two phase detector outputs, one output using the carrier I input and the other output using the carrier Q input, as shown

in Fig. 5. When tracking the subcarrier and/or symbol loop while the carrier is open-loop demodulated, and when the symbol SNR is low, using two arms provides a 3-dB gain in the loop SNR as the signals in both channels are used. When the carrier is in lock, no additional information and only additional noise is gained by using the second channel and, therefore, a conventional one-arm loop is used.
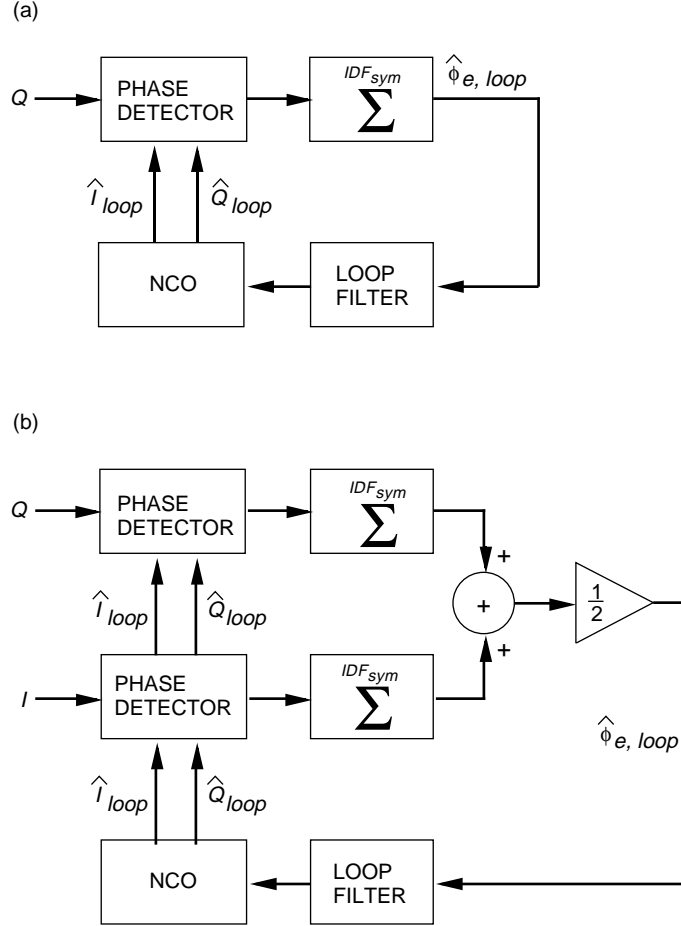

Fig. 5. Subcarrier or symbol tracking loops: (a) one arm and (b) two arm.

C. Initial Bandwidths and Windows

When FFT acquisition is complete, each estimate of signal phase and frequency will have associated with it a variance, $\sigma^2_{\phi,FFT}$ and $\sigma^2_{f,FFT}$, respectively (given in the last section). The initial tracking loop bandwidth (and transition window if applicable) is chosen by matching the loop phase variance, σ^2_ϕ, with the FFT-estimated phase variance, $\sigma^2_{\phi,FFT}$. This is analogous to a constant-bandwidth tracking loop handing over to the acquisition loops, which will start at the bandwidth and window and begin narrowing.

The tracking variance σ^2_ϕ for each type of loop can be written in the form

$$\sigma^2_\phi = \begin{cases} (2\pi)^2 c^2_\phi B_L w \ \ \text{rad}^2, & \text{for loops with transition windows (SCL and SSL)} \\ (2\pi)^2 c^2_\phi B_L \ \ \text{rad}^2, & \text{otherwise (suppressed carrier loop)} \end{cases}$$

where B_L is the loop noise bandwidth, w is the window width size, and c_ϕ^2 is a constant that depends on the signal SNR and the tracking loop. For loops with transition windows, the window is specified in terms of the tracking variance with the parameter c_w:

$$w = \frac{c_w \sigma_\phi}{(2\pi)}$$

$$c_w = \begin{cases} 4c_w', & \text{for subcarrier loops} \\ 2c_w', & \text{for symbol loops} \end{cases}$$

The parameterization of c_w in terms of c_w' is for physical significance: c_w' gives the tracking error that reaches the edge of the transition window, expressed in tracking standard deviations. For example, with $c_w' = 4$, the (unlikely) tracking error of $4\sigma_\phi$ is necessary to cause the signal transition to fall outside of the phase extractor window.

We can now solve for the initial bandwidth and window width:

$$w(0) = \frac{c_w \sigma_{\phi,FFT}}{2\pi}$$

$$B_L(0) = \frac{\sigma_{\phi,FFT}^2}{(2\pi)^2 c_\phi^2 w(0)}$$

For a loop with no transition window, the initial bandwidth is

$$B_L(0) = \frac{\sigma_{\phi,FFT}^2}{(2\pi)^2 c_\phi^2}$$

The windowing allows the initial bandwidth to be w times larger than with no windowing for a given loop SNR.

D. Bandwidth and Window Narrowing

In the continuous bandwidth and window narrowing methods used,[6] the loop time constant $\tau \triangleq 1/(2B_L)$ is linearly increasing in time with rate $d\tau/dt$. Bandwidth as a function of time then has the form

$$B_L(t) = \frac{1}{2\left(\frac{1}{2B_L(0)} + \frac{d\tau}{dt}t\right)} \tag{40}$$

In tracking loops with transition windows, window as a function of time is given by

$$w(t) = w(0)\frac{B_L(t)}{B_L(0)}$$

---

[6] The bandwidth and window narrowing method is introduced and analyzed in S. Stephens, "Bandwidth and Window Modification in Phase-locked Loops," JPL Interoffice Memorandum 335.9-94-010 (internal document), Jet Propulsion Laboratory, Pasadena, California, June 1994.

From simulation[7] and analysis, values of $d\tau/dt$ and c'_w that minimize the loop phase variance after a fixed time span are specified for loops[8] of order N and damping parameter η^2 and are given in Table 1.

Table 1. Optimum values of $d\tau/dt$ and c'_ω for loops of order N and damping parameter η^2.

Loop	$d\tau/dt$	c'_w
Subcarrier loop, $N = 2, \eta^2 = -1$	0.181	4.0
Symbol loop, $N = 1$	1.0	4.0
Symbol loop, $N = 2, \eta^2 = -1$	0.181	4.0
Carrier loop, $N = 2, \eta^2 = -1$	0.383	

From solving Eq. (40), the time, T_{fin}, to reach $B_{L,fin}$ from $B_L(0)$ is

$$T_{fin} \;=\; \frac{1}{2\frac{d\tau}{dt}}\left(\frac{1}{B_{L,fin}} - \frac{1}{B_L(0)}\right) \;\approx\; \frac{1}{2\frac{d\tau}{dt}B_{L,fin}} \tag{41}$$

Note that for $d\tau/dt = 0.181$,

$$T_{fin} \approx \frac{2.8}{B_{L,fin}}\ \text{sec}$$

For digital loops, bandwidth and window width values can be changed no faster than the update rate. Processor limitations may impose an even tighter constraint: for the Block V Receiver, the loop parameters may only be modified once per second. If the continuous equations above are used to generate discrete values of bandwidths and windows at rates (f_u) much larger than the loop bandwidth, then the analysis should still hold; this is confirmed by simulation in Section VI. However, if f_u is comparable to or larger than the loop bandwidth, the analysis in Footnote 6 specifies a maximum allowable change in the value per update time of $1/f_u$ sec. In this case, the bandwidths and windows are narrowed in the limited step sizes allowed per update time. For Galileo fast-acquisition in the BVR ($f_u = 1$ Hz), where the bandwidths are less than $f_u = 1$ Hz for all loops, we can always use the continuous approximation.

The bandwidth function versus time is illustrated in Fig. 6(a). The dark line shows the actual bandwidth values applied to the tracking loop. The steps reflect the update rate $f_u = 1$ Hz, at which the bandwidth is modified. The following sections discuss $B_{L,min}$ and $B_{L,fin}$.

The window function versus time is illustrated in Fig. 6(b). The dark line shows the actual window width values applied to the tracking loop. The limitation of the window value (in the BVR) to a 2^{-n} value (discussed in Section V) results in quantized window values, as in the figure. A discussion of w_{fin} and w'_{fin} follows.

---

[7] The implementation and simulation of Footnote 6 is discussed in M. Aung, S. Stephens, and C. Buu to J. Berner, "Block V Receiver Implementation and Simulation of Bandwidth and Window Narrowing Methods in [1]," JPL Interoffice Memorandum 3338-94-042 (internal document), Jet Propulsion Laboratory, Pasadena, California, June 3, 1994.

[8] S. A. Stephens and J. B. Thomas, "First-Principles Analysis of Digital Phase-Locked Loops with Controlled-Roots, Transient-Response-Specific Parameterization," JPL Interoffice Memorandum 335.1-91-032 (internal document), Jet Propulsion Laboratory, Pasadena, California, November 22, 1991.
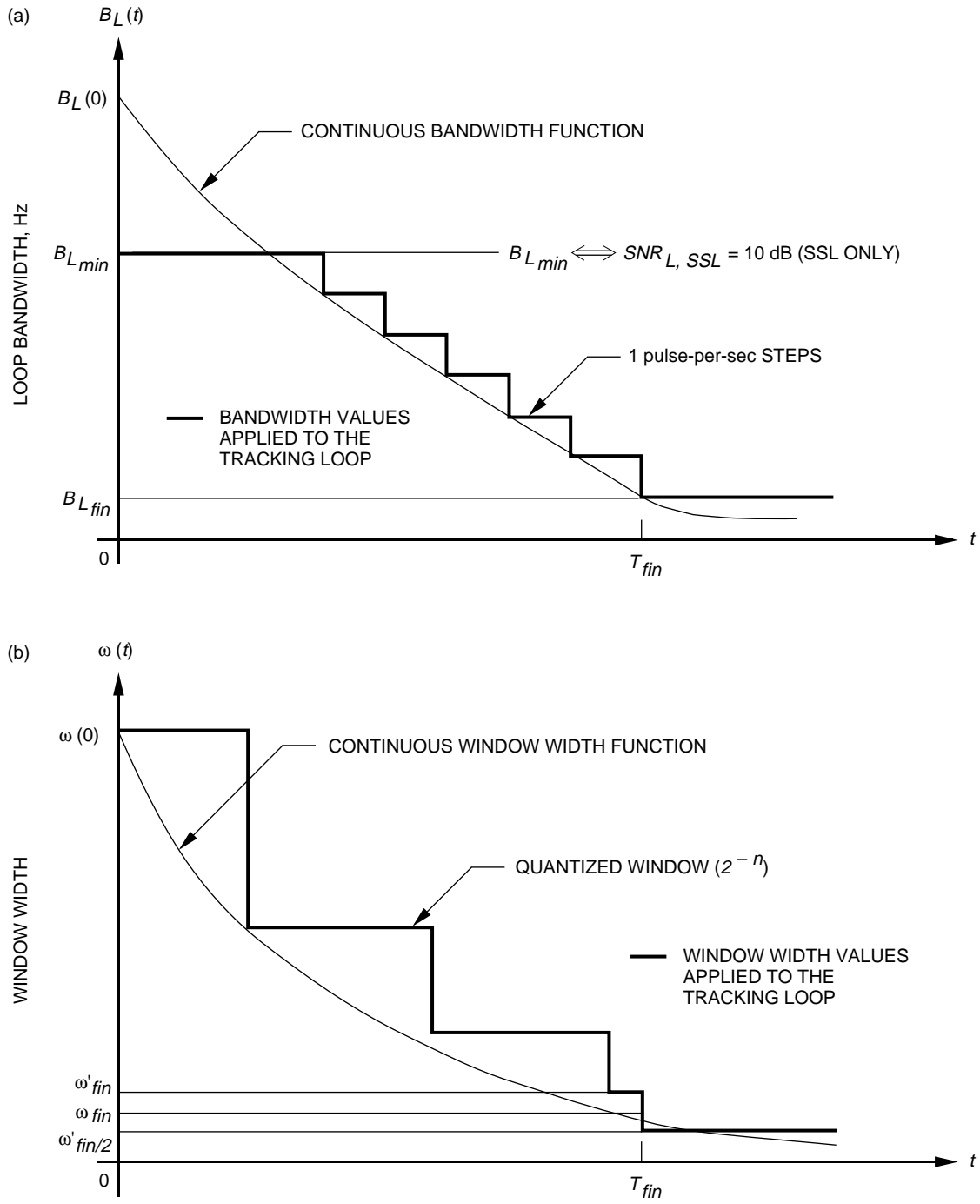
Fig. 6. Bandwidth and window narrowing: (a) loop bandwidth versus time *t* and (b) $\omega(t)$ versus time *t*.

E. Final Bandwidths and Windows

The final bandwidth, $B_{L,fin}$, is determined from a specified maximum output symbol SNR loss; the bandwidth narrowing routine stops narrowing when it reaches the final required bandwidth at time $t = T_{fin}$. However, window quantization will cause the final quantized window value w'_{fin} to be larger than w_{fin}, specified by the continuous equations above. This in turn yields a lower final loop SNR

than desired. For compensation, the window or bandwidth must be narrowed an additional amount. During narrowing, the tracking variance at any given time can be twice as large as that implied by the bandwidth alone, due to transients in the narrowing process. Thus, the optimum windowing factor c'_w during narrowing will be larger than the factor used once narrowing transients have died away. The method implemented for reaching the final design loop SNR makes use of this smaller c'_w when the narrowing process is completed; the window is narrowed by an additional factor of two at the end of the narrowing process, which is when the final bandwidth is reached, as shown in Fig. 6(b), i.e., at $t = T_{fin}$, the window is set to $w'_{fin}/2$.

F. Special Considerations

For the symbol loop, the initial bandwidth specified above may cause the initial loop SNR of the SSL to be somewhat low (e.g., when $SNR_{FFT} = 12$ dB and symbol phase is estimated from a set of subcarrier acquisition FFTs (Section III.B.2), the initial SSL SNR is about 8 dB). For this case, the bandwidth is limited to $B_{L,min}$, which corresponds to a loop SNR of 10 dB; the window width calculation uses the continuous bandwidth function before it is limited, so that the window is kept larger for transients caused by the narrow bandwidth [Fig. 6(a)].

V. Implementation in the Block V Receiver

The fast acquisition algorithm has been implemented in the BVR; this section discusses the issues regarding its implementation. The BVR high-speed digital signal-processing hardware consists of five application-specific integrated circuits (ASICs) that are used to demodulate the carrier and up to two subcarriers and two symbol streams. There are three unique ASIC designs: carrier processing, subcarrier processing, and symbol processing. The two telemetry processing channels (subcarrier and symbol loops) are provided by independent sets of the subcarrier and symbol ASICs, each set receiving the in-phase (I) and quadrature-phase (Q) carrier demodulation outputs (the subcarrier ASIC can internally reverse the I and Q inputs). All tracking loop NCOs are frequency and phase updatable. The software processing of each telemetry channel is also independent of the other.

Implementation of the fast acquisition algorithm involved changing the software tasking structure of the BVR subcarrier and symbol tracking loops and modifying the algorithm for the software implementation. The carrier, subcarrier, and symbol tracking loops are implemented as independent software tasks. As such, the loop acquisitions are independent processes; it is possible to acquire the subcarrier and symbol loops sequentially or simultaneously. The fast acquisition algorithm requires that the subcarrier and symbol loops be controlled together. To accomplish this, a separate task was created for the fast acquisition process. The subcarrier and symbol loops have two acquisition tasks each, the normal acquisition, which is independent for each loop, and the fast acquisition, which controls both loops.

Upon receipt of the acquisition command, the task zeroes out the subcarrier and symbol NCO phases and sets the subcarrier NCO frequency to the predicted subcarrier frequency and the symbol NCO frequency to the predicted symbol rate times $N_{sc,acq}$. The subcarrier reference signal type is set to sine wave (as opposed to the normal square wave). Because there are no accumulators to sum the symbol integration outputs, the symbols must be read into software for processing. This means that the symbol NCO frequency used must be less than the symbol hardware interrupt rate (1 or 2 kHz). This places a limit on the product of $N_{sc,acq}$ and the symbol rate. For this part of the acquisition process, only one set of telemetry ASICs is used, since all four outputs (II, IQ, QI, and QQ) are available.

The FFT size is determined from the input predicted signal parameters. The data are collected, and the complex subcarrier FFT inputs for the $N_{sc,acq}$ FFTs are generated. A Sky Computer Skybolt array processor board is used to compute the FFTs, which can be as large as 2^{17} points. After the (subcarrier, symbol, and carrier) phase and frequency are estimated from the FFT acquisition, the tracking loop

NCOs, which are frequency and phase updatable, are initialized with the FFT-estimated values, and the loops are closed. The subcarrier reference signal type is changed to the square wave.

If the carrier loop has not yet been acquired, the subcarrier and symbol loops must be operated in the two-arm mode. This uses both sets of telemetry ASICs to generate the windowed subcarrier and symbol tracking loop inputs (the second set of ASICs has the I and Q inputs reversed, providing the needed signals to give windowed versions of the II, IQ, QI, and QQ signals). If the carrier is locked, only one telemetry channel is required.

The implementation of the transition window-narrowing and bandwidth-narrowing algorithms also required some trade-offs, due both to hardware and software concerns. The subcarrier and symbol windows are implemented in the ASICs and are quantized to a factor of two. In other words, the hardware window widths are step selectable in increments of 2^{-n}, where n is an integer in the range of 0 to 15. So, the algorithm could not continuously vary the window width; it had to quantize the windows to the hardware capabilities.

The update rates of the narrowing algorithms (both window and bandwidth) were also quantized in time. All tracking loops have two update rates: the hardware interrupt rate, which is the rate that the software reads in the data off of the ASICs and processes the tracking loop, and the once-per-second pulse, which is the rate at which the performance data are reported and the loop configuration parameters are updated. It was determined that the narrowing algorithms could be updated at the lower rate (once per second), which allowed a simpler implementation that did not require lowering the interrupt rate (the higher the interrupt rate, the less time there is to process the software instructions required to close the loop).

VI. Computer Simulation

Extensive computer simulations were performed to verify the design and analysis of the fast acquisition method.[9] The simulations examine the following aspects of the fast acquisition algorithm:

(1) Subcarrier FFT acquisition

(2) Symbol FFT acquisition

(3) Carrier FFT acquisition

(4) Subcarrier, symbol, and carrier loop acquisition

In order to verify case 1 [step (1) of Figs. 2 and 3], the subcarrier FFT acquisition is simulated in the presence of demodulation errors, and the resulting frequency and phase estimates are compared to the input parameters. The theoretical performance of the algorithm is also evaluated in terms of the probability of FFT detection and statistics on the frequency and phase estimates. Specifically, the simulations verify agreement between measured and predicted values for the following:

(1a) Subcarrier tone SNR when the symbol rate error is negligible and the subcarrier is acquired using four initial symbol phase offsets

(1b) Subcarrier tone SNR when the symbol rate error is significant

---

[9] References for the simulation results are summarized in M. Aung to E. W. Stone, "Computer Simulation Work Supporting the Design and Analysis of the Block V Receiver Fast Acquisition Algorithm," JPL Interoffice Memorandum 3338-94-053 (internal document), Jet Propulsion Laboratory, Pasadena, California, June 1, 1994, which gives an overview of the simulation work and lists all interoffice memoranda reporting the simulation results.

(1c) FFT detection confidence

(1d) Subcarrier frequency and phase estimates

(1e) Subcarrier frequency and phase estimate variances

Verification of (1e) is important since the SCL is closed with the initial bandwidth, and the window values are calculated as functions of the predicted standard deviation of the FFT-estimated phase. In addition, (1a) and (1d) were verified for actual Galileo downlink data recorded at Goldstone. Good agreement to within one or two standard deviations of the measured value was seen for (1a), (1b), (1d), and (1e). For (1c), an approximate predict was used, resulting in some divergence with the simulated value.

In symbol FFT acquisition, when the error in the predicted symbol frequency is negligible, the symbol phase can be estimated from the subcarrier acquisition by interpolating the $N_{sc,acq}$ PSDs of the subcarrier FFT acquisition. If the symbol phase detection fails due to a symbol rate error, the symbol frequency and phase are acquired via FFT methods. Hence, for steps (4), (10), and (11) of Fig. 2 and steps (4), (9), and (10) of Fig. 3, the simulations verify agreement between measured and predicted values for the following:

(2a) Symbol phase when the symbol rate error is negligible and the phase is estimated from the four subcarrier acquisition FFTs

(2b) Symbol phase estimate variances for (2a)

(2c) Symbol frequency and phase and the variances of these estimates when the symbol rate is unknown

(2d) Symbol error tone SNR when the symbol rate is unknown

Verification of variance of the FFT estimate is important since the SSL is closed with the initial bandwidth and window values, which are calculated as functions of the predicted standard deviation of the FFT-estimated phase. For (2a) through (2d), good agreement to within one or two standard deviations of the measured value was seen. Agreement varied slightly for (2b), but the uncertainty lies in the computation of the predicted standard deviation (an approximation of the true standard deviation was used).

Simulations of the subcarrier and carrier simultaneous FFT acquisition [step (1), Fig. 3] confirm that carrier FFT acquisition is analogous to subcarrier FFT acquisition in terms of tone SNRs. Therefore, results obtained for case (1) can be applied to case (3).

The loop acquisition in case (4) was simulated separately by initializing the loop NCO phase and frequency with errors equal to one standard deviation of the FFT estimates. The loops are then closed with initial bandwidths and window widths as described in Section IV.C. The bandwidths are narrowed as described in Section IV.D until the desired symbol SNR degradation is achieved. The window widths are narrowed in quantized increments of 2^{-n} to reflect hardware implementation constraints in the BVR. In addition, the simulation update rate of the narrowing algorithm is set to 1 pulse per sec in accordance with the BVR loop configuration parameter update rate. The simulations measure acquisition times for the following cases:

(4a) The subcarrier, symbol, and carrier loops are closed simultaneously using the one-arm approach [steps (5) through (7) in Fig. 3].

(4b) The two-arm SCL and SSL are closed, followed by carrier FFT acquisition first and then the carrier loop acquisition [steps (5) through (8) in Fig. 2]. This is simulated by closing all three loops simultaneously, assuming that the carrier FFT acquisition time is negligible compared to the SCL and SSL loop acquisition times.

(4c) The two-arm SCL and SSL are closed while the carrier loop is left open [steps (5) and (6) in Fig. 2].

Good agreement is observed between measured and predicted acquisition times as discussed in Section VII.

VII. Acquisition Times

The acquisition time of the fast acquisition algorithm is defined as the length of time required until all the loops (subcarrier, symbol, and carrier if applicable) have attained loop SNRs high enough to contribute only a tolerable amount of degradation to the output symbol SNR. For the high carrier phase-noise case (Section II.A) when the carrier is acquired after the subcarrier and symbol acquisition, the acquisition time is

$$T_{acq} = MAX\{T_{sc,acq}, T_{sym,acq}\} + T_{carr,acq} \text{ sec} \tag{42}$$

where $T_{Y,acq}$ ($Y = sc$, sym, or $carr$, indicating subcarrier, symbol or carrier) is the acquisition time of the indicated signal. For the low carrier phase-noise case (Section II.B) when the subcarrier, symbol, and carrier are acquired simultaneously, the acquisition time is

$$T_{acq} = MAX\{T_{sc,acq}, T_{sym,acq}, T_{carr,acq}\} \text{ sec} \tag{43}$$

In the following, individual acquisition times for the subcarrier, symbol, and suppressed carrier ($T_{sc,acq}$, $T_{sym,acq}$, and $T_{carr,acq}$, respectively) are presented. For each case, $T_{Y,acq}$ is defined as

$$T_{Y,acq} = T_{Y,FFT} + T_{Y,loop} \tag{44}$$

where $T_{Y,FFT}$ is the FFT acquisition time and $T_{Y,loop}$ is the loop acquisition time.

The FFT acquisition time, $T_{Y,FFT}$, is

$$T_{Y,FFT} = N_{data}T_{sym} = \frac{SNR_{Y,FFT}}{E_s^*/N_o}T_{sym} \tag{45}$$

where $SNR_{Y,FFT}$ is the SNR in the FFT-acquisition of the signal under consideration.

The loop acquisition time for each loop, $T_{Y,loop}$, is defined as the length of time for narrowing the bandwidth and window width until the design loop SNR, $SNR_{L,fin}$, is achieved. The $SNR_{L,fin}$ is determined by the maximum allowed degradation, $Deg(\phi)$, to the output symbol SNR due to the loop phase jitter, ϕ. The relationships between $Deg(\phi)$ and ϕ are listed in Table 2 for the SSL, SCL, and the suppressed carrier loop. The expected degradation, $\overline{Deg(\phi)}$, calculated as the statistical expectation of $Deg(\phi)$ assuming a Gaussian distribution for ϕ, is also listed in Table 2 where $SNR_L \triangleq 1/\sigma_\phi^2$.

Table 2. Degradation, *Deg(φ)*, to the output symbol SNR due to loop phase error φ, and expected values of *Deg(φ)* and $\overline{Deg(\phi)}$ for the SCL, SSL, and carrier loops.

Loop	$Deg(\phi)$	$\overline{Deg(\phi)}$
SCL	$\left(1 - 4\frac{|\phi|}{2\pi}\right)^2$	$1 - 8\sqrt{\frac{1}{2SNR_L\pi^3}} + \frac{4}{SNR_L\pi^2}$
SSL	$\frac{1}{2}\left(1 + \left(1 - 2\frac{|\phi|}{2\pi}\right)^2\right)$	$1 - 4\sqrt{\frac{1}{SNR_L(2\pi)^3}} + \frac{2}{SNR_L(2\pi)^2}$
Suppressed carrier loop	$\cos^2(\phi)$	$\frac{1}{2}\left(1 + e^{-\frac{2}{SNR_L}}\right)$

The $SNR_{L,fin}$ is calculated as the minimum SNR_L required for a given expected degradation. In Table 3, $SNR_{L,fin}$ is calculated for expected degradation values of $\{0.1, 0.2, 0.5, 1\}$ dB, i.e., for final degradation of $\{0.1, 0.2, 0.5, 1\}$ dB to the output symbol SNR due to each loop, the loop bandwidth and window width are to be narrowed until the loop SNR of $SNR_{L,fin}$ of Table 3 is achieved. When designing for low final loop SNRs, the $SNR_{L,fin}$ derived should be padded conservatively, e.g., by 1 dB, to compensate for nonlinear effects not modeled in the equations used for loop SNRs.

Table 3. Minimum required loop SNRs, *SNR_{L,fin}*'s, as a function of $\overline{Deg(\phi)}$.

$\overline{Deg(\phi)}$, dB	SCL $SNR_{L,fin}$, dB	SSL $SNR_{L,fin}$, dB	Suppressed carrier loop $SNR_{L,fin}$, db
0.1	33	21	16
0.2	27	15	13
0.5	19	6.5	9
1.0	13.0	0	6

Recall that the initial loop SNR is set equal to $1/\sigma^2_{\phi_{FFT}}$, the inverse of the variance of the FFT-estimated phase at the time the loop is closed. For the acquisition time plots presented in this section, it is assumed that SNR_{FFT} is 12 dB, and that the tracking loop is closed at $t_{cl,loop} = T_{FFT}$. In this case, the initial SNR_L's are listed in Table 4. For the SSL, $1/\sigma^2_{\phi_{FFT}}$ is less than the minimum loop SNR of 10 dB required to avoid cycle slipping; therefore, the loop will be started with a bandwidth such that the initial loop SNR is 10 dB, as described in Section IV.F. By comparing Tables 3 and 4, it is seen that the carrier loop starts out very close to or above the $SNR_{L,fin}$ required. Hence, the carrier loop acquisition time is essentially 0, leaving only the FFT acquisition time. As larger degradations to the output symbol SNR are tolerated, the required $SNR_{L,fin}$ are smaller and the loop acquisition times are shorter. In fact, for a degradation of 0.5 dB, the loop acquisition times for both the symbol and the suppressed carrier are 0 sec, leaving only the FFT acquisition time. For a 1-dB degradation, the loop acquisition time is 0 for all three loops.

The loop acquisition time, $T_{Y,loop}$, is calculated as the time to reach the required final bandwidth, $B_{L,fin}$, corresponding to the required $SNR_{L,fin}$, Eq. (41), plus $1/2B_{L,fin}$ sec. The latter term is an approximation of the additional time the loop transients will require to die out after the final window narrowing by an extra factor of two at the end of the narrowing process (Section IV.E). Hence,

$$T_{loop} = \frac{1}{2(d\tau/dt)} \left(\frac{1}{B_{L,fin}} - \frac{1}{B_{L,init}} \right) + \frac{1}{2B_{L,fin}} \qquad (46)$$

where

$$B_{L,fin} = \begin{cases} \dfrac{1}{c_w c_\phi^2} \dfrac{1}{\sqrt{SNR_{L,fin}}} \dfrac{1}{2\pi} & \text{SCL and SSL} \\[2ex] \dfrac{1}{c_\phi^2 SNR_{L,fin}(2\pi)^2} & \text{suppressed carrier loop} \end{cases}$$

and

$$B_{L,init} = \begin{cases} \dfrac{1}{2\pi} \dfrac{\sigma_{\phi_{FFT}}}{c_w c_\phi^2} & \text{SCL and SSL} \\[2ex] \dfrac{\sigma_{\phi_{FFT}}^2}{c_\phi^2(2\pi)^2} & \text{suppressed carrier loop} \end{cases}$$

Table 4. Initial loop SNRs when $SNR_{FFT} = 12$ dB.

Loop	$SNR_{L,init} = 1/\sigma_{\phi_{FFT}}^2$, dB
SCL	14.8
SSL (symbol phase estimation by interpolation)	8 (10 dB used to avoid cycle slips)
SSL (FFT frequency and phase estimation)	8.8 (10 dB used to avoid cycle slips)
Suppressed carrier loop	14.8

Acquisition times vary with the types of loops: one-arm versus two-arm and different loop orders.[10] In this section, $T_{sc,acq}$, $T_{sym,acq}$, and $T_{carr,acq}$ are presented for the high carrier phase-noise case. In Figs. 7(a), 8(a), and 9(a), $T_{sc,acq}$ is plotted for final degradations of 0.1, 0.2, and 0.5 dB, respectively. Similarly, in Figs. 7(b), 8(b), and 9(b), $T_{sym,acq}$ is plotted. The suppressed carrier acquisition time plotted in Fig. 7(c) is presented as $T_{carr,acq} = T_{carr,FFT}$ (with the assumption that $T_{carr,loop} \approx 0$ sec) for final degradations of 0.1, 0.2, and 0.5 dB.

In these figures, $T_{Y,acq}$ is a function of P_D/N_o and E_s/N_o (or R_{sym}). Hence, families of curves of $T_{Y,acq}$ versus P_D/N_o are plotted for various values of E_s/N_o. Note the decrease in the acquisition times for larger final degradations.

The total acquisition time of the algorithm, T_{acq}, for the final degradation of 0.1, 0.2, or 0.5 dB from each loop, is estimated as in Eq. (41). For example, for $P_D/N_o = 14.6$ dB-Hz and $R_{sym} = 16$ symbols per sec ($E_s/N_o = 2.56$ dB) expected when the Galileo spacecraft is at JOI, the acquisition time, $T_{acq,JOI}$, for a final degradation of 0.2 dB is

$$T_{acq,JOI} = MAX\{26.4, 33.1\} + 5.9 = 38 \text{ sec}$$

---

[10] A complete set of acquisition times for the different loops is in C. Buu, S. Stephens, and M. Aung to J. Berner, "Acquisition Times of the Fast Acquisition Algorithm," JPL Interoffice Memorandum 3338-94-052 (internal document), Jet Propulsion Laboratory, Pasadena, California, June 4, 1994.
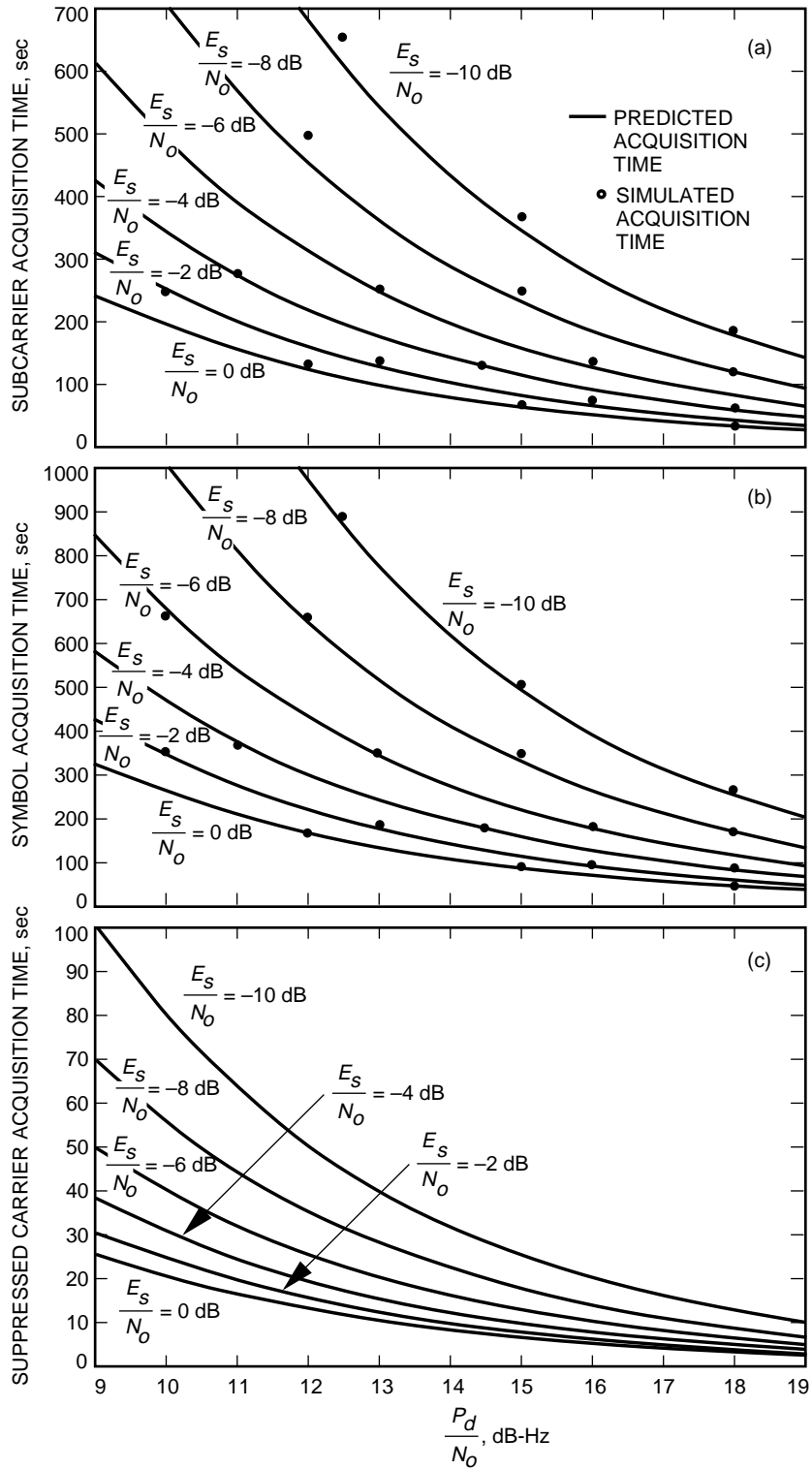
Fig. 7. Acquisition time to reach 0.1-dB degradation in output symbol SNR due to phase jitter in each loop: (a) subcarrier $T_{sc,acq}$, and (b) symbol $T_{sym,acq}$, and for (c) suppressed carrier $T_{carr,acq}$ to reach 0.1, 0.2, or 0.5–dB degradation.

The simulated acquisition times are also included in Figs. 7–9, shown in discrete points. In the simulations, $SNR_{L,fin}$ padded by 1 dB was used. Relatively good agreement is seen between the predicted and the simulated times. The seemingly larger divergence in the plots for a 0.5-dB degradation is largely due to the vertical scale of the plot. In Figs. 7(c) and 9(b), no simulation points are included as $T_{acq} = T_{FFT}$.
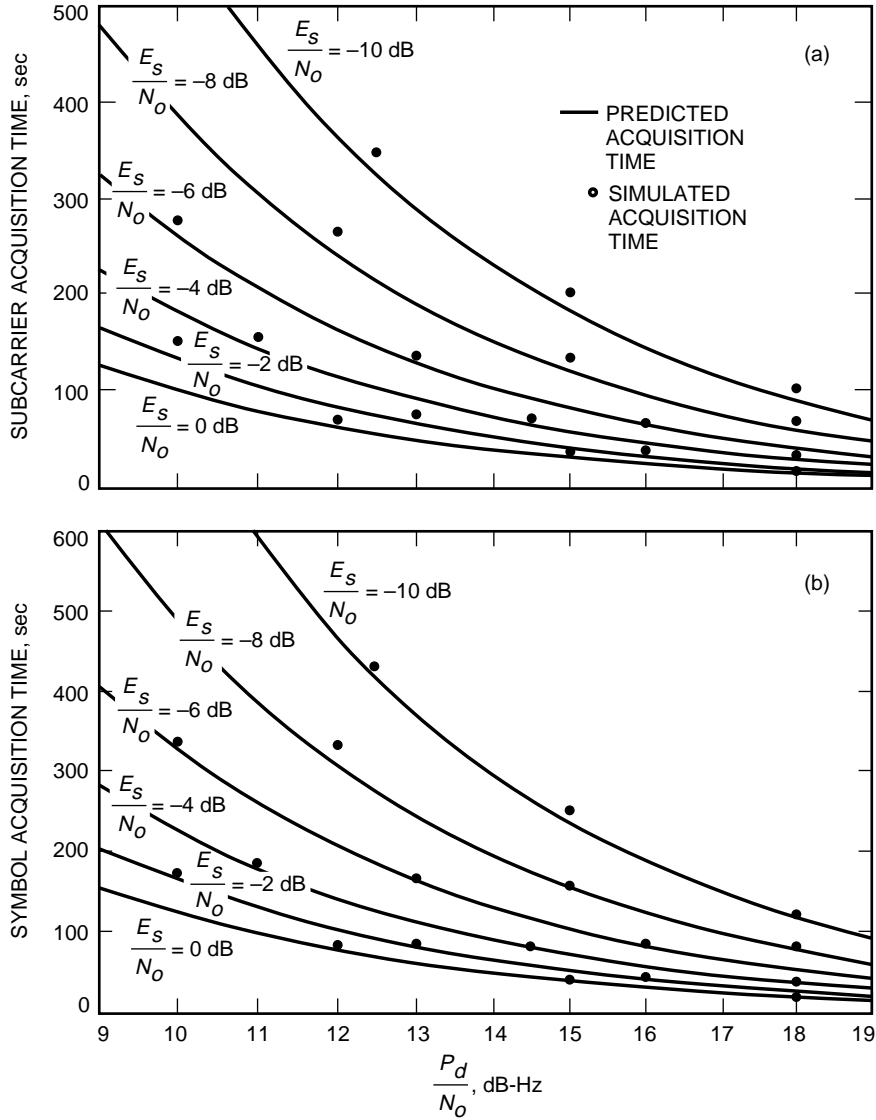

Fig. 8. Acquisition time to reach 0.2-dB degradation in the output SNR due to phase jitter in each loop: (a) subcarrier $T_{sc,\ acq}$ and (b) symbol $T_{sym,\ acq}$.

VIII. Conclusion

The fast acquisition algorithm developed for the Galileo S-band mission that is expected to encounter low data rate, low SNR, and high carrier phase-noise conditions is presented in this article. Multiple schemes resulting in faster acquisition times are introduced. Implementation of the algorithm in the Block V Receiver is described. Simulation work supporting the algorithm is discussed. Finally, the acquisition times of the algorithm are presented. In the expected case for the Galileo spacecraft at

JOI ($P_D/N_o = 14.6$ dB-Hz and $R_{sym} = 16$ symbols per sec), the acquisition time to attain a 0.2-dB degradation from each loop to the output symbol SNR is estimated to be 38 sec.
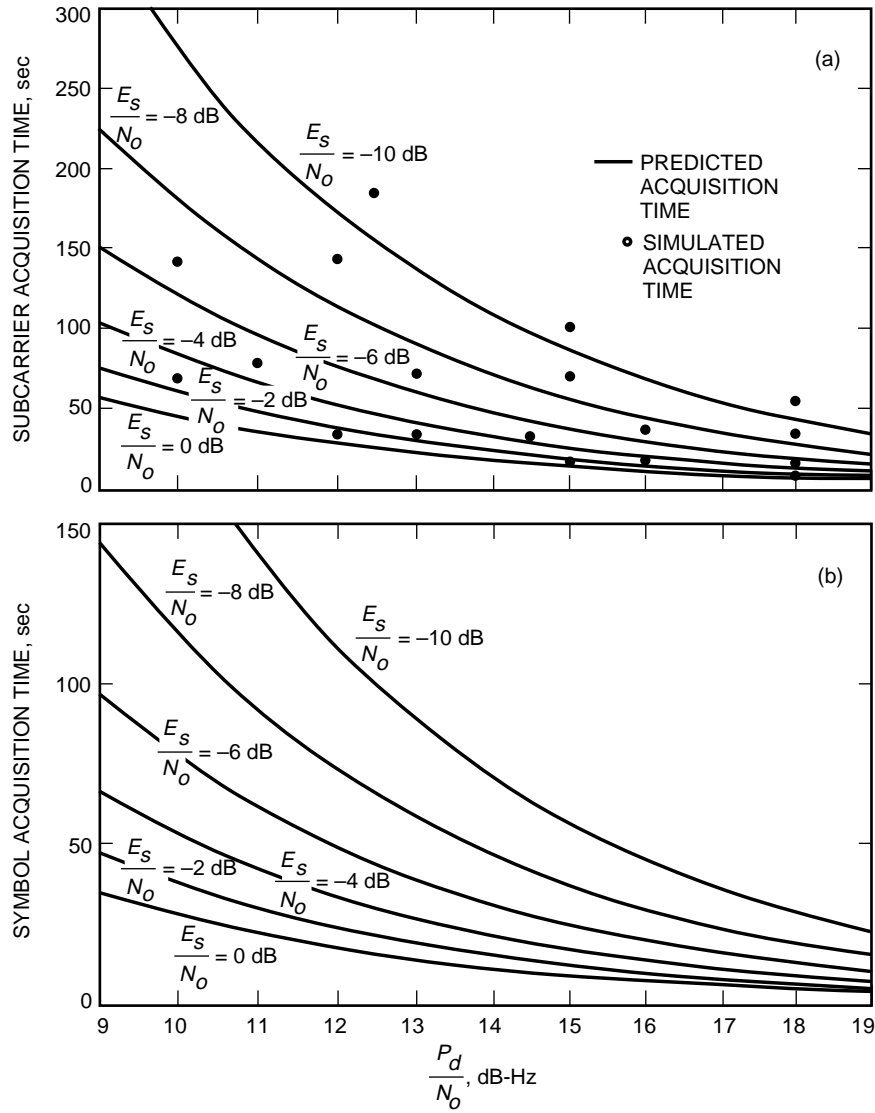

Fig. 9. Acquisition time to reach 0.5-dB degradation in the output symbol SNR due to phase jitter in each loop: (a) subcarrier $T_{sc,\,acq}$ and (b) symbol $T_{sym,\,acq}$.

Acknowledgments

References

[1] J. Berner and K. Ware, "An Extremely Sensitive Digital Receiver for Deep Space Satellite," *Eleventh Annual International Phoenix Conference on Computers and Communications 1992 Proceedings*, Scottsdale, Arizona, pp. 577–585, April 1–3, 1992.

[2] W. J. Hurd and S. Aguirre, "A Method to Dramatically Improve Subcarrier Tracking," *The Telecommunications and Data Acquisition Progress Report 42-86, vol. April–June 1986*, Jet Propulsion Laboratory, Pasadena, California, pp. 103–110, August 15, 1986.

Appendix

Frequency Interpolation and Phase Estimation From the FFT

In this appendix, the technique adopted for estimation of the frequency and phase of an exponential tone from its FFT is discussed. Expressing the input exponential tone signal, $s(m)$, sampled every $T_{s,FFT}$ sec as

$$s(m) = Ae^{j(2\pi f_{in}t + \phi_o)} \mid_{t=mT_{s,FFT}} \tag{A-1}$$

the technique for estimating the frequency and phase (f_{in} and ϕ_o, respectively) is described.

A. Frequency Estimation Using Sinc Interpolation

An N_{FFT}-point complex FFT of the signal $s(m)$ will have a peak at bin number k_{peak}. By interpolation between the complex FFT values of the peak bin and two bins about the peak, n bins away, the frequency f_{in} can be estimated as $\hat{f}_{FFT}$. The interpolation assumes an underlying sinc function relation between the three points (rather than a simple quadratic one), resulting in an improved estimate of frequency. The interpolated FFT estimate, $\hat{f}_{FFT}$, is

$$\hat{f}_{FFT} = \frac{k_{peak} + \Delta k}{N_{FFT}} \frac{1}{T_{s,FFT}}$$

where

$$\Delta k = \text{frequency bin interpolation}$$
$$k_{peak} = \text{bin number of the peak tone}$$
$$N_{FFT} = \text{FFT size}$$
$$T_{s,FFT} = \text{FFT sampling time}$$

The Δk is calculated as

$$\Delta k = n \times Re \left[\frac{\gamma Z_{(k_{peak}+n)_{mod N_{FFT}}} + \gamma^* Z_{(k_{peak}-n)_{mod N_{FFT}}}}{\gamma Z_{(k_{peak}+n)_{mod N_{FFT}}} - \gamma^* Z_{(k_{peak}-n)_{mod N_{FFT}}} + (\gamma^* - \gamma) Z_{k_{peak}}} \right] \qquad \text{(A-2)}$$

where

$Z_k = $ complex FFT value of the kth bin

$\gamma = e^{j2\pi n/\alpha} - 1$

$\alpha = \dfrac{N_{FFT}}{N_{data}}$

$\quad = $ zero-padding factor, may not be an integer

$n = MAX \left\{ Floor\left[\dfrac{\alpha}{2}\right], 1 \right\}$

When $\alpha = 1$, Eq. (A-2) becomes in the limit

$$\Delta k = Re \left[\frac{Z_{(k_{peak}+1)_{mod N_{FFT}}} - Z_{(k_{peak}-1)_{mod N_{FFT}}}}{Z_{(k_{peak}+1)_{mod N_{FFT}}} + Z_{(k_{peak}-1)_{mod N_{FFT}}} - 2Z_{k_{peak}}} \right] \qquad \text{(A-3)}$$

B. Phase Estimation

The phase ϕ_o of the signal at $t = 0$ can be estimated from its FFT as $\hat{\phi}_{FFT}$:

$$\hat{\phi}_{FFT} = \Delta\hat{\phi}_{FFT} - 2\pi \hat{f}_{FFT} \frac{T_{s,FFT}}{2} \qquad \text{(A-4)}$$

where

$$\Delta\hat{\phi}_{FFT} = Arg\ \left[Z_{k_{peak}}\right] - 2\pi\Delta k \frac{(N_{data} - 1)}{2\alpha N_{data}} \qquad \text{(A-5)}$$

and $T_{s,FFT}$ is the sample rate of the FFT input signal.